# PID Controller for Blowdown Supersonic Wind Tunnel

a project presented to
The Faculty of the Department of Aerospace Engineering
San José State University

in partial fulfillment of the requirements for the degree
*Master of Science in Aerospace Engineering*

by

## Yu Ting Huang

December 2021

approved by

Dr. Maria Chierichetti
Dr. Fabrizio Vergine
Faculty Advisor

# ABSTRACT

## PID Controller for Blowdown Supersonic Wind Tunnel

Yu Ting Huang

The objective of this research is to design a reliable Proportional-Integral-Derivative (PID) controller to safely and effectively control the plenum chamber stagnation pressures during Mach 2 tests for the blowdown supersonic wind tunnel (BSWT) at SJSU. The progress of the project developments is divided into four phases.

In phase I, a simplified mathematical model of the pressure valve opening area is established to provide a theoretical preview of the valve dynamics; hence justifying the need for a PID controller in conjunction with a valve booster. In phase II, a governing differential equation that directly relates the valve opening angle to the plenum chamber pressure difference and the controller is formulated. Following that, a numerical algorithm that incorporates the mass flow rate of the specific commercial valve used at SJSU is developed to process the valve and pressure dynamics. In phase III, The physical BSWT is virtually constructed by using Simscape$^{TM}$ libraries in the Simulink$^{TM}$ environment. Finally, in phase IV, PID controller gains are first obtained from the second method of Ziegler-Nichols rules and later on fine-tuned to achieve 1 % pressure percent error for both the numerical algorithm and the Simscape-BSWT model. Implementing the same selected optimal PID controller gains, both the numerical solution and the simulation from the virtual plant model are generated and discussed regarding the rise time and run time.

# ACKNOWLEDGEMENTS

# TABLE OF CONTENTS

# LIST OF TABLES

# LIST OF FIGURES

Chapter 6

# NOMENCLATURE

$A^*_{1_{est}}(d)$   =   Estimated variable cross-sectional area at throat 1 as a function of distance

$A^*_{1_{est}}(t)$   =   Estimated variable cross-sectional area at throat 1 as a function of time

$A^*_{1_{est}}(\theta_{time})$   =   Estimated variable cross-sectional area at throat 1 as a function of angle-time array

$A^*_{1_{est}}(\theta)$   =   Estimated variable cross-sectional area at throat 1 as a function of driveshaft turning angle

$A^*_1(t)$   =   Variable cross-sectional area at throat 1 as a function of time

$A^*_2$   =   Fixed cross-sectional area at throat 2

$A_{TS}$   =   Cross-sectional area of the test section

$a^*_1$   =   Speed of sound at throat 1

a2Star   =   Fixed cross-sectional area at throat 2

$C_G$   =   Gas sizing coefficient

$C_v$   =   Flow coefficient of the valve at rated travel

$C_1$   =   Valve recovery coefficient

$d_{max}$   =   Maximum distance between the centers of the two congruent circles

$\dfrac{d^2 P_{p,i}}{dt^2}$   **=**   Initial acceleration of plenum chamber pressure

$E(s)$   =   Actuating error term in the complex domain

$G_c(s)$   =   Transfer function in the complex domain

GAMMA   =   Ratio of specific heats for a calorically perfect gas

$h_v$   =   Specific enthalpy of the air going through the control valve

$I(s)$   =   Control input in the complex domain

$I(t)$   =   Control input in the time domain

$K_D$   =   Derivative controller

$K_I$   =   Integral controller

$K_P$   =   Proportional controller

$M^*_1$   =   Mach number at throat 1

$M^*_2$   =   Mach number at throat 2

$\dot{m}$   =   Constant mass flow rate

| | | |
|---|---|---|
| $\dot{m}_v$ | = | Mass flow rate of the valve |
| $\dot{m}_1$ | = | Constant mass flow rate at throat 1 |
| $\dot{m}_2$ | = | Constant mass flow rate at throat 2 |
| $\dot{m}_2^*$ | = | Mass flow rate through throat 2 |
| $M_{TS}$ | = | Mach number in the test section |
| $O(s)$ | = | Control output in the complex domain |
| $O(t)$ | = | Control output in the time domain |
| $P_P$ | = | Total pressure in the plenum chamber |
| $P_{P,i}$ | = | Initial plenum chamber pressure |
| $P_P(s)$ | = | Sensing feedback of plenum chamber pressure in the complex domain |
| $P_P(t)$ | = | Sensing feedback of plenum chamber pressure in the time domain |
| $P_{pd}(s)$ | = | Desired plenum chamber pressure in the complex domain |
| $P_{T_{initial}}$ | = | Initial total tank pressure |
| $P_{T,i}$ | = | Initial total tank pressure |
| $P_2^*$ | = | Static pressure at throat 2 |
| $P_2$ | = | Static pressure at throat 2 in the isentropic relationship |
| point | = | Evenly spaced points |
| $P_T(t)$ | = | Total pressure in the tank as a function of time |
| $P_{TS}$ | = | Total pressure in the test section |
| $Q_{SCFH}$ | = | Volumetric flow rate at standard conditions |
| $R$ | = | Specific gas constant |
| $R$ | = | Radius of congruent circles |
| $T_P$ | = | Total temperature in the plenum chamber |
| $T_T$ | = | Total temperature in the tank |
| $T_2^*$ | = | Static temperature at throat 2 |
| $T_2$ | = | Static temperature at throat 2 in the isentropic relationship |
| $T_d$ | = | Derivative controller |
| $T_i$ | = | Integral controller |

| | | |
|---|---|---|
| TO | = | Total temperature |
| $V_P$ | = | Volume of the plenum chamber |
| $V_T$ | = | Volume of the tank |
| $v_v$ | = | Velocity of the air going through the control valve |
| VOL_PL | = | Volume of the plenum chamber |
| VOL_TK | = | Volume of the tank |
| $X_T$ | = | Manufacturer coefficient |
| $\gamma$ | = | Ratio of specific heats for a calorically perfect gas |
| $\theta_{ini}$ | = | Initial valve opening angle at time 0 |
| $\theta$ | = | Angle of rotation of the valve |
| $\theta_i$ | = | Initial valve angle |
| $\theta_{time}$ | = | Angle-time array |
| $\theta(s)$ | = | Valve angle in the complex domain |
| $\theta(t)$ | = | Valve angle in the time domain |
| $\rho_1^*(t)$ | = | Density at throat 1 as a function of time |
| $\rho_2^*$ | = | Density at throat 2 |
| $\rho_T$ | = | Total density in the tank |
| $\rho_T(t)$ | = | Total density in the tank as a function of time |

# Chapter 1 - Introduction

## 1.1 Motivation

Blowdown Supersonic Wind Tunnels (BSWTs) that can deliver uniform supersonic flow with desired similarity parameters (Mach number & Reynolds number) are critical to the analysis of the aerodynamics of a test subject in a laboratory environment [1]. During a test of blowdown wind tunnels, a flow that is discharged from a high-pressure tank to a plenum chamber travels continuously to a test section and finally leaves the wind tunnel from a diffuser. According to the isentropic flow theory, a desired Mach in the test section can be attended by one of the flow characteristics such as pressure, density, or temperature ratio of the total condition over the static condition between the inlet and outlet of the test section. The geometry between the cross-sectional area and the throat can be determined with the desired Mach number. Figure 1.1 depicts the schematic diagram of a typical supersonic blowdown wind tunnel.
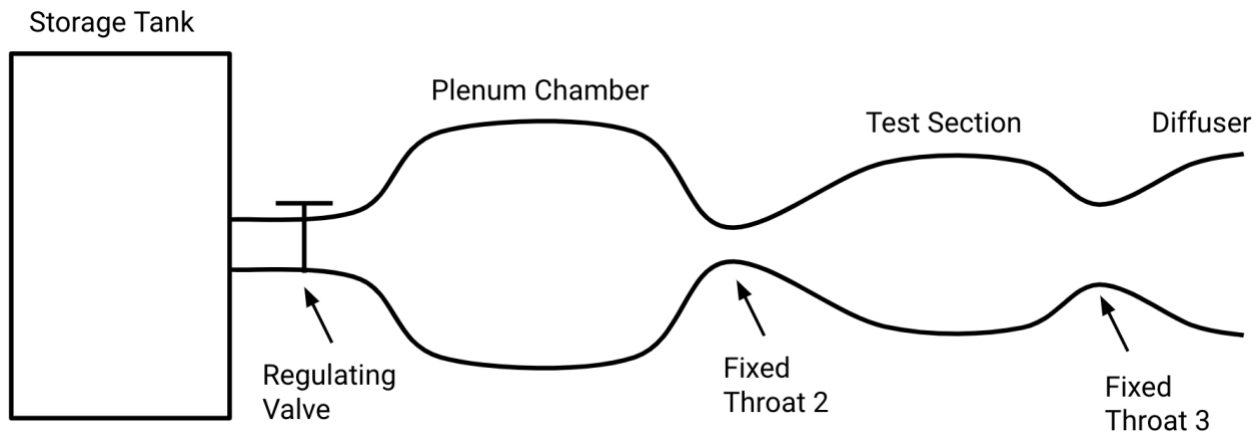


Figure 1. 1 Schematic diagram of a typical blowdown supersonic wind tunnel

A constant total condition in the test section such as stagnation pressure that does not vary in space and time is imperative for a successful wind tunnel test. The control of constant stagnation pressure is usually handled by one or more pressure regulators after the storage tank [2]. During a test, the regulator valve will be opened up gradually to let the high-pressure flow from the storage tank to the plenum chamber whose total pressure is considered to be equal to the total pressure in the test section. Thus, it is necessary to control the dynamics of the valve opening so that the constant stagnation pressure in the test section can be maintained.

With the growth of computing power, managing the valve dynamics has become more and more effective and efficient since the first supersonic wind tunnels in the mid-1930s. Despite the automation advantages, there remain several challenges in terms of the control of flow parameters and most of them are related to the control of total pressure during a wind tunnel test [3]. Since the operation cost of wind tunnels is high and the pressurized air storage is limited [4], it is favorable to complete a run that fulfills requirements for measurement quality as fast as possible. A PC-based pre-programmed controller developed by Lu and Matsumoto can reduce the pressure disturbance in the plenum chamber to one percent of the desired total pressure with a short run time, but several attempts are required to optimize the controller for a test section Mach [5]. In addition, a sudden change in operating conditions will result in a poor transient

response of the Mach number and the stagnation pressure in the test section [6]. Moreover, failure to adjust the varying stagnation pressure and mass flow can induce dangerous pressure oscillation in the plenum chamber, which is known as "organ piping" [2][7].

The applications of this research will directly contribute to the operation of the supersonic blowdown wind tunnel for the Aerospace Engineering Department at San Jose State University. In addition, the findings from this project will also contribute to the literature for the future.

A control system should respond fast enough to accommodate the fast pressure drop of the storage tank so as to maintain constant total pressure in the test section. Most controllers of pressure regulators for supersonic wind tunnels proposed in the literature did not look into the acceleration of the valve opening speed. The purpose of this project, therefore, is to develop a reliable Proportional-Integral-Derivative (PID) controller to effectively control the opening of the pressure regulating valve so as to maintain constant plenum chamber stagnation pressures for supersonic blowdown wind tunnels in a Simulink environment.

## 1.2 Literature Review

This section provides a literature review regarding the existing proposed solutions to the control of the stagnation pressure in the settling chamber of supersonic blowdown wind tunnels. Pressure regulators play an important role in terms of the runtime and energy consumption of BSWTs [4]. The purpose of controlling the opening of the pressure regulating valve is to maintain constant total pressures in the test section during blowdown runs. There are many ways to establish the rules for valve opening angle. In general, research activities have been tackling the problem from two main different perspectives: statistical methods and physical model-based methods. The following three subsections will briefly describe the research from these two approaches respectively and the Ziegler-Nichols tuning technique.

### 1.2.1 Statistical Approach

The most obvious advantage of the statistical approach is that it can train the algorithm to work for complex models without knowing every detail or the mathematical model of the system. When mathematical models are too difficult to obtain, experimental approaches or Artificial Neural Networks (ANNs) can be used to describe the plant dynamics [8]. After systems are defined, the designed controllers can be optimized even for non-linear multivariable systems by modern controllers tuning techniques, such as Genetic Algorithms (GA) and Fuzzy Logic Controller(FLC) [9].

Motter and Principe [10] from NASA Langley Research Center used Kohonen self-organizing feature maps [11] to cluster the local tunnel dynamics that was built from ANN and to predict the Mach response to control inputs [10] [11]. Nott et al. [12] at the University of Alabama designed a gain scheduled PID controller from an ANN model that captures the wind tunnel characteristics, uncertainties, sensor dynamics, and time delays. The controller was then optimized for fast rise time to the steady-state on that ANN model using GA [12]. Since the proposed controller described in [12] was to be applicable over a range of operating conditions, the design process was re-iterated over various throat settings to acquire the pattern of the controller gains.

2

In addition to system representation, ANN can also be used to find desired controller gains. For instance, in [13], the optimal membership functions of the  FLC system for valve opening angle in various operation conditions were determined by ANN after the establishment of a nonlinear mathematical model of the BSWT.  This scheme shows several advantages; it can reduce harmful emissions, maximize run time, minimize operation noise,  improve the safety of the system, and reduce running costs. Although these techniques can yield high fidelity to the flow control parameters, tuning controllers without considering the physical properties of the wind tunnel flow tend to be convoluted during the training step [14].

Other than the aforementioned approaches, an ideal valve opening profile can also be established from experimental data alone. Lu and Matsumoto[15] designed a rapid valve opening technique for a BSWT from test data. In a feedforward sense, the pre-programmed controller was pre-loaded with a valve opening schedule obtained from the prior run with the same test condition. Through several training runs and corrections, the valve opening angle could be calibrated to keep the plenum chamber pressure constant [15]. The most significant of this type of controller is that the impacts from input time delays and slow react devices can be diminished. Furthermore, it can start a BSWT very fast without overshooting the plenum chamber pressure. The downsides are that several training runs are required to idealize the controller and it may fail to account for disturbances due to the lack of feedback signals.

1.2.2 Physical Model-Based Approach

Contrary to the statistical approach, the physical model-based method design suitable controllers based on the physical properties of the flow in the wind tunnel [14]. Due to non-ideal gas behaviors, sensor dynamics, pressure regulating valve dynamics, characteristics of storage and plenum chambers, etc., most supersonic blow-down wind tunnels are complex and non-linear systems [15] [1]. Therefore, assumptions are usually brought in to simplify the complex system when modeling BSWT and isentropic flow is often used as the basic assumption to simplify mathematical models.

Hwang et al [15] developed a lumped-component mathematical model by assuming a sonic condition in the control valve for blowdown wind tunnels and designed an LQG/LTR controller to minimize the effects of uncertainties mentioned above [15] [1].

In [2], a simple PI controller was developed to keep the plenum chamber stagnation pressure constant for a BSWT at the University of Texas Arlington in a LabVIEW environment. Since the total pressure is the only feature to be controlled, Braun et al. chose a proportional-integral (PI) controller to control the valve opening. Figure 1.2 shows the block diagram of their designed PI controller for the operation of the BSWT.

3
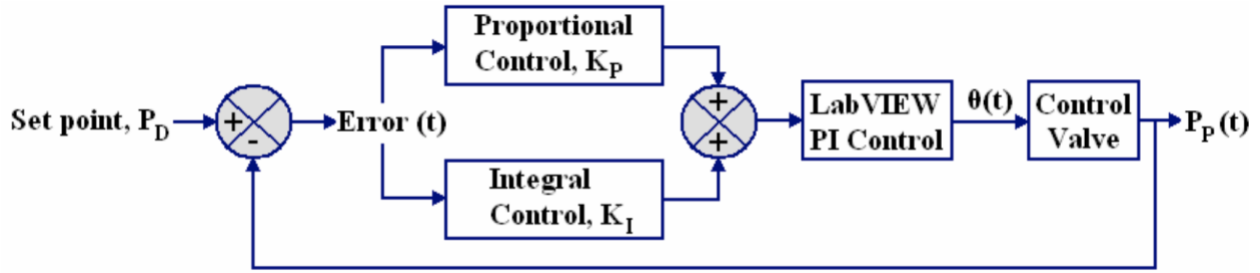
Figure 1. 2 Block diagram of PI controller [2]

Here the reference value, $P_D$, is a desired plenum chamber pressure, whereas the output $P_P$ is the results obtained from either the simulation or LabVIEW. The error between $P_D$ & $P_P$ is then handled by a tuned PI controller to control the angle of the valve. Although the valve opening angle was obtained numerically, the $K_P$ and $K_I$ had to be manually tuned throughout a simulated blowdown run. After the simulation, Braun et al. built the LabVIEW$^{TM}$ controller based on the same governing differential equation used from the simulation but with real-time measurements of thermocouple, pressure transducer, and valve angle to compute the valve angle. Although the design is straightforward, the controlled plenum chamber pressure has undesirable overshoot and long rise time [3].

To enhance the controller performance proposed by [2], Corneliu came up with a scheme that consisted of a PI controller, a reference model, and an FLC [16] and implemented the system in Simulink. The resulting performance of [16] was benchmarked against the experimental data collected from INCAS BSWT and showed improvement in faster rise time and less overshoot.

In [14], the lumped parameter [17] mathematical model that represented the VTI T-38 BSWT (Figure 1.3) was developed. This highly nonlinear model mainly due to the gas dynamics and the control valve characteristics was applied to the BSWT to obtain the non-linear information about the facility. The essential information was then feedback to Simulink models of the facility. Finally, the proposed controller was tuned to manage the desired total pressure during a wind tunnel test. This feedforward-feedback control method [18] was validated with the facility experiments and had shown improvement in terms of both disturbance rejection and setpoint tracking.
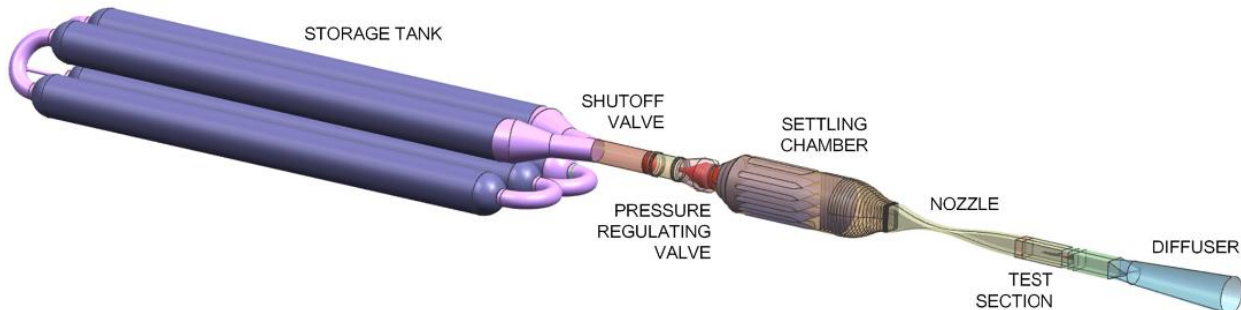


Figure 1. 3 VTI BSWT [3]

### 1.2.3 Ziegler-Nichols Tuning Rules

Among many other offline controller tuning rules, such as Cohen-Coon method or Chien-Hrones-Reswick autotuning, the Ziegler-Nichols method has been widely used for determining the values of control parameters since its publication in 1942 [19][20][21]. Ziegler-Nichols tuning method gains its popularity because it is easy to use and it provides a good starting point for calibration [22]. In addition, when the mathematical model of the plant is unknown, controller gains and important parameters can still be obtained experimentally. Despite its usefulness, it causes overshoot in the transient state and it can be applied to single-input-single-output (SISO) systems only [9]. Two types of Ziegler-Nichols tuning rules will be described in the following subsections to show how to obtain the values of the control parameters proportional gain $K_p$, integral time $T_i$, and derivative time $T_d$. Figure 1.4 is the block diagram of a closed-loop system with a PID controller.



**Set Point** → $E(s)$ → $K_p \left( 1 + \frac{1}{T_i s} + T_d s \right)$ → $U(s)$ → **Plant** → **Process Output**
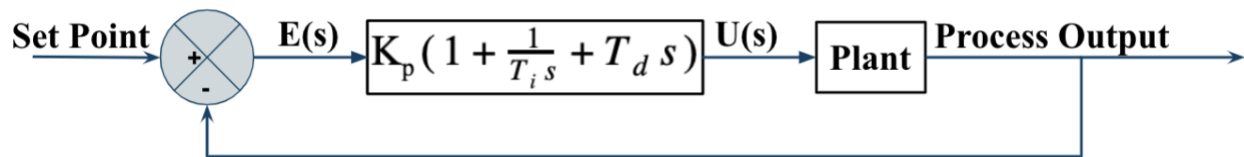
Figure 1. 4 PID control of a plant in s-domain

### 1.2.3.1 Method 1

The first method is applicable when the plant does not have complex conjugate poles nor integrators [22]. The technique of method 1 considers the system output, c(t), to the unit-step input, u(t), in the time domain. From the unit-step response of a system, two constants can be obtained: delay time L and time constant T. Both constants are determined by the origin, the tangent line at the inflection point of the plant response curve, and the intersection points of the tangent line with the t-axis as well as with the unit-step-input line (see Figure 1.5). After obtaining both constant L and T, one can refer to the Ziegler-Nichols tuning table (Table 1.1) to determine the values for $K_p$, $T_i$, and $T_d$ when designing the controllers.
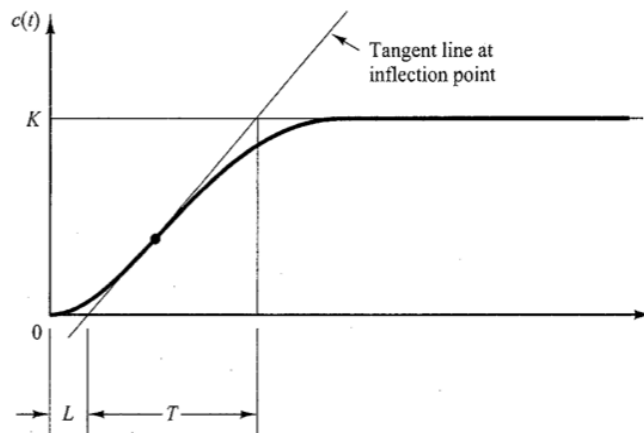


Figure 1. 5 Unit-step response [22]

*Table 1. 1 Ziegler-Nichols tuning table (method 1)[22]*

| Type of Controller | $K_p$ | $T_i$ | $T_d$ |
|---|---|---|---|
| P | $\dfrac{T}{L}$ | $\infty$ | 0 |
| PI | $0.9\dfrac{T}{L}$ | $\dfrac{L}{0.3}$ | 0 |
| PID | $1.2\dfrac{T}{L}$ | $2L$ | $0.5L$ |

1.2.3.2 Method 2

The second method involves a critical value $K_{cr}$ gain and the corresponding critical period $P_{cr}$. Under a closed-loop system setup (Figure 1.6), to obtain the value of $P_{cr}$, we set $T_i = \infty$ and $T_d = 0$, and increase $K_p$ from 0 to a value that results in a steady oscillation output (Figure 1.7). The value of $K_p$ that causes the steady oscillation is the $K_{cr}$. Together with the acquired period $P_{cr}$, the values of $K_p$, $T_i$, and $T_d$ from the Ziegler-Nichols tuning table (Table 1.2) can be used to determine the control parameters [22]. Since $K_{cr}$ represents the gain for marginal stability of an open-loop transfer function of the plant, $K_{cr}$ and $P_{cr}$ can also be obtained from the steady frequency $\omega_{cr}$ from the root-locus scheme when the mathematical model of the plant is known [22].
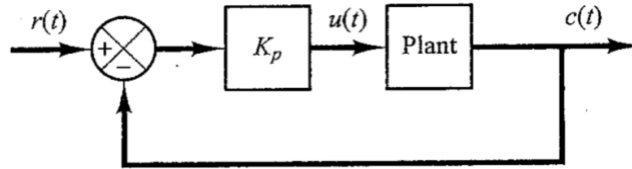


Figure 1. 6 Closed-loop system in the time domain
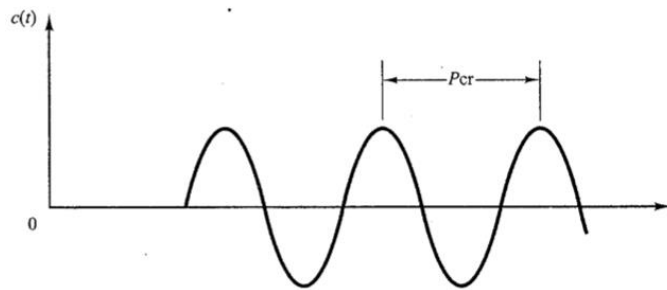


Figure 1. 7 Steady-state output [22]

*Table 1. 2 Ziegler-Nichols tuning table (method 2)[22]*

| Type of Controller | $K_p$ | $T_i$ | $T_d$ |
|---|---|---|---|
| P | $0.5K_{cr}$ | $\infty$ | 0 |
| PI | $0.45K_{cr}$ | $\dfrac{1}{1.2}P_{cr}$ | 0 |
| PID | $0.6K_{cr}$ | $0.5P_{cr}$ | $0.125P_{cr}$ |

## 1.3 Project Proposal

The objective of this research is to develop a reliable control system to safely and effectively control the plenum chamber stagnation pressures during blowdown runs of the supersonic wind tunnels at San Jose State University (SJSU). From the literature review, it is believed that a PID controller first tuned by the second method of Ziegler-Nichols rules is suitable to control the pressure valve dynamics that have a direct impact on providing a uniform test environment.

## 1.4 Methodology

The approaches to achieve the project objective described in section 1.3 can be divided into four phases:

- Phase I - Preliminary study:
  Based on the assumption of compressible, isentropic flow in the tunnel, a mathematical model that represents the physical system of the pressure valve will be developed.
- Phase II - PID controller and the governing equation:
  A governing equation that relates the pressure regulating valve, the evolution of plenum chamber pressure, and the PID controller will be derived. Based on the governing equation, an algorithm will be devised to numerically integrate the derivative terms to obtain the time-variant pressure valve profile and plenum chamber pressure.
- Phase III - Modeling system dynamics in Simulink$^{TM}$:
  The physical BSWT will be virtually constructed by using Simscape$^{TM}$ libraries in the Simulink$^{TM}$ environment.
- Phase IV - Numerical solution and simulation:
  The numerical solution and the simulation from the Simscape-BSWT model will be generated and compared with the tuned PID controller.

Figure 1.8 graphically shows the progress of the project. Note that the project progress is an iterative process. If the discrepancies between the numerical solution and the simulation in Phase IV are beyond a reasonable range, models in Phase II and Phase III will need to be fixed, or the underlying assumptions in Phase I will need to be re-investigated to better address the problem at hand.
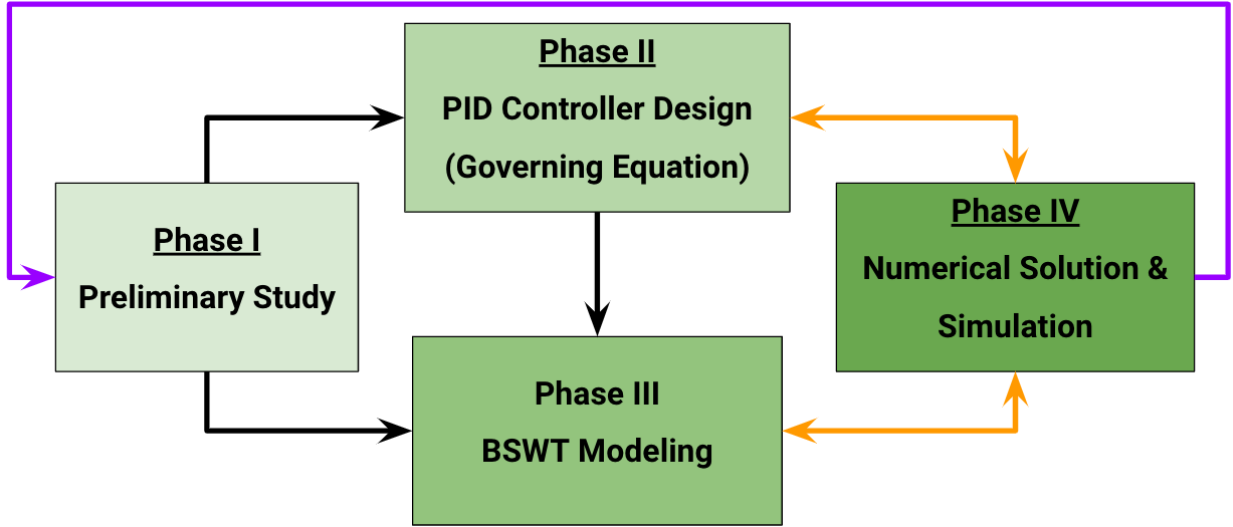
Figure 1. 8 Structure of the concept progress

# Chapter 2 - Preliminary Analysis

## 2.1 Overview of Controller Design Development

The pressure PID controller design for the BSWT is described in different chapters in the following orders:
- Mathematical modeling of the valve dynamics (chapter 2)
- PID controller design (chapter 3)
- Computational solution of the process dynamics (chapter 4)
- Simscape modeling of BSWT (chapter 5)
- Tuning and validation of PID controller (chapter 6)

In this chapter, the mathematical model of a throat area in the BSWT will be developed based on the law of conservation of mass, with the assumption of compressible, isentropic flow in the tunnel. An estimated solution for the valve opening area will also be developed to determine the initial valve open angle needed right at the beginning of an experiment. Chapter 2 will be concluded by mapping the estimated solution to the analytical solution before a PID controller is installed. In chapter 3, a brief overview of PID controllers will be introduced and a governing differential equation that relates the tank pressure, valve opening angle, the plenum chamber stagnation pressure, and the control constants will be developed. Following the developed governing equation, an algorithm that performs numerical integration will be schemed to solve the state variables, namely valve opening angle, plenum chamber stagnation pressure, and tank stagnation pressure. In chapter 4, the computational solutions performed by both numerical algorithms and Simulink will be used to validate the mathematical modeling of the controlled system. In chapter 5, the physical BSWT will be modeled by using Simscape libraries in the Simulink environment. In chapter 6, the second method of Ziegler-Nichols tuning rules will be first carried out to obtain the base set of gain constants. The virtual BSWT response will be satisfied by further fine-tuning of the control gains. Finally, with the implementation of the selected set of optimal controller gains on the virtual BSWT, the numerical solution and the computational simulation will be compared to validate the PID controller design.

## 2.2 Mathematical Modeling of the Valve Dynamics

The objective of the designed PID controller is to maintain a constant plenum chamber stagnation pressure while the total pressure in the tank is decreasing during blowdown runs. During a blowdown run, the pressure regulating valve, which is the actuating device for a pressure control BSWT, will be opened up progressively. Thus, how much the valve should be opened right at the beginning and during an experiment should be investigated first. For mathematical representation, the valve dynamics that will be modeled is the cross-sectional area of the valve opening.

### 2.2.1 Analytical Solution of the Cross-Sectional Area at throat 1

Extending the schematic diagram of the BSWT shown in Figure 1.1, important parameters needed (see Table 2.1) for determining the PID controller gain are added to the diagram shown in Figure 2.1:

*Table 2. 1 Summary of the essential parameters for the BSWT*

| Parameter | Description | Unit (SI) |
|---|---|---|
| $P_T(t)$ | Total pressure at the tank as a function of time | Pa |
| $\rho_T(t)$ | Total density at the tank as a function of time | kg/m³ |
| $T_T$ | Total temperature at the tank | K |
| $V_T$ | Volume of the tank | m³ |
| $a*_1$ | Speed of sound at throat 1 | m/s |
| $\rho*_1(t)$ | Density at throat 1 as a function of time | kg/m³ |
| $M*_1$ | Mach number at throat 1 | - |
| $A*_1(t)$ | Variable cross-sectional area at throat 1 as a function of time | m² |
| $P_P$ | Total pressure in the plenum chamber | Pa |
| $\rho*_2$ | Density at throat 2 | kg/m³ |
| $M*_2$ | Mach number at throat 2 | - |
| $A*_2$ | Cross sectional area at throat 2 | m³ |
| $P_{TS}$ | Total pressure in the test section | Pa |
| $M_{TS}$ | Mach number in the test section | - |
| $A_{TS}$ | Cross sectional area in the test section | m³ |
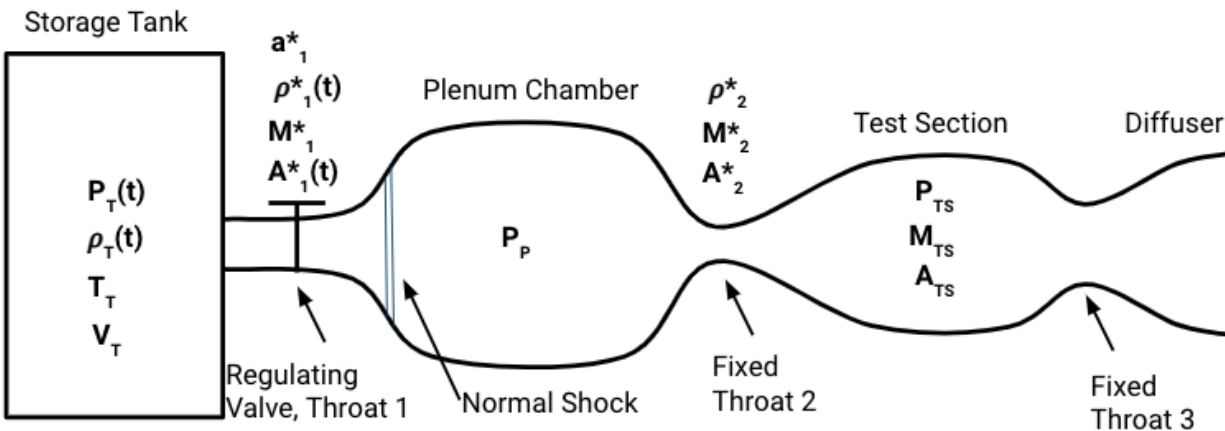


Figure 2. 1 Schematic diagram of a BSWT with essential parameters

The assumptions for the mathematical modeling are:

- Flow is choked at throats
- Viscous effects are neglected in compressible flow
- Flow in the tunnel during blowdown tests is isentropic before and after the normal shock
- Perfectly expanded supersonic nozzle

By control volume analysis, the mass flow rate is constant throughout:

$$\dot{m} = constant$$
$$= \dot{m}_2 = \dot{m}_1$$
$$= \rho_1^*(t)a_1^*M_1^*A_1^*(t)$$

$$(2.1)$$

Rearrange equation (3.1), we get:

$$A_1^*(t) = \frac{\dot{m}_1}{\rho_1^*(t)a_1^*M_1^*}$$

$$(2.2)$$

Assuming flow is choke at throat 1, equation (2.2) is reduced to:

$$A_1^*(t) = \frac{\dot{m}_1}{\rho_1^*(t)a_1^*}$$

$$(2.3)$$

The details of each term $\dot{m}_1$, $\rho_1^*(t)$, and $a_1^*$ in equation (2.3) will be derived respectively in the following subsections. In subsection 2.2.1.4, these three terms will be reassembled in MATLAB to plot equations (2.3) and (2.11) so as to verify if the derivation of equations has been done correctly.

2.2.1.1 Derivation of the Mass Flow Rate at Throat 1

Decompose each term in equation (2.3), the numerator term $\dot{m}_1$ or the mass flow rate at throat 1 becomes:

$$\dot{m}_1 = \rho_2^*\sqrt{\gamma R T_2^*}A_2^*$$

$$(2.4)$$

where $\gamma$ is the ratio of specific heats for a calorically perfect gas, $R$ is the specific gas constant, and T*$_2$ is the static temperature at throat 2.

From the equation of state for a perfect gas [1], $p = \rho RT$, $\rho_2^*$ becomes:

$$\rho_2^* = \frac{p_2^*}{RT_2^*} \tag{2.5}$$

Since the flow is isentropic, the static pressure at throat 2 can be derived from the isentropic relationship between the static and total condition. Similarly, the static temperature at throat 2 can also be obtained from the isentropic relationship by setting $T_p = T_T$ even though there is a presence of a normal shock after throat 1, i.e. total temperature remains constant across the shock [23].

Assuming flow is choke at throat 2, i.e. $M_2^* = 1$, the static pressure and temperature become:

$$p_2^* = p_p \frac{p_2}{p_p}$$

$$= p_p[(1 + \frac{\gamma - 1}{2}M_2^{*2})^{\frac{\gamma}{\gamma-1}}]^{-1}$$

$$= p_p[(1 + \frac{\gamma - 1}{2})^{\frac{\gamma}{\gamma-1}}]^{-1} \tag{2.6}$$

$$T_2^* = T_T \frac{T_2}{T_T}$$

$$= T_T[(1 + \frac{\gamma - 1}{2}M_2^{*2})]^{-1}$$

$$= T_T[(1 + \frac{\gamma - 1}{2})]^{-1} \tag{2.7}$$

The fixed throat area A*2 is obtained from the Area-Mach number relation [1]:

$$(\frac{A_{TS}}{A_2^*})^2 = \frac{1}{M_{TS}^2}[\frac{2}{\gamma + 1}(1 + \frac{\gamma - 1}{2})M_{TS}^2]^{\frac{\gamma+1}{\gamma-1}} \tag{2.8}$$

Rearrange equation (2.8) and the designed $A^*_2$ becomes:

$$A^*_2 = \frac{A_{TS}}{\sqrt{\frac{1}{M^2_{TS}}[\frac{2}{\gamma+1}(1+\frac{\gamma-1}{2})M^2_{TS}]^{\frac{\gamma+1}{\gamma-1}}}}$$

(2.9)

2.2.1.2 Derivation of the Density at Throat 1

The first term $\rho^*_1(t)$, the density at throat 1, in the denominator of equation (2.3) is equal to the static density of the tank $\rho^*_T$ and can be obtained from the equation of state and isentropic relationship again:

$$\rho^*_1(t) = \rho_T \frac{\rho^*_T}{\rho_T} = \frac{P_T(t)}{RT_T} \frac{\rho^*_T}{\rho_T}$$

(2.10)

where the total tank pressure as a function of time can be derived from subtracting the decreasing total tank pressure during a test from the initial total tank pressure:

$$p_T(t) = P_{T_{initial}} - \frac{\dot{m}_1 \bullet lapse}{V_T} RT_T$$

(2.11)

The lapse term in equation (2.11) is the passage of test time between 0 ~ test duration. This time array must have the same number of evenly spaced points as the turn angle $\theta$ in computation for one-to-one mapping later described in section 2.3.3. Also, note that the final total tank pressure or the lowest total tank pressure at the end of a blowdown test is equal to the desired total plenum chamber pressure, the test duration can be obtained from rearranging equation (2.11) and setting $P_T(t) = P_p$:

$$duration = \frac{(P_{T_{initial}} - p_p)V_T}{RT_T \dot{m}_1}$$

(2.12)

13

## 2.2.1.3 Derivation of the Speed of the Sound at Throat 1

Finally, since the flow is isentropic, the speed of the sound for a calorically perfect gas [1] at throat 1 when the flow is choked can be derived from the following equation and this constant value is found to be 313.7531 m/s:

$$
\begin{aligned}
a_1^* &= \sqrt{\gamma R T_1^*} \\
&= \sqrt{\gamma R T_T [(1 + \frac{\gamma - 1}{2} M_1^{*2})]^{-1}} \\
&= \sqrt{\gamma R T_T [(1 + \frac{\gamma - 1}{2})]^{-1}}
\end{aligned}
$$

$$(2.13)$$

## 2.2.1.4 Plot the Valve Opening at Throat 1

Taking all the equations described above and substituting in given parameter values (see table 2.2), a MATLAB algorithm was developed (Appendix C) to calculate and plot the evolution of the total pressure in the tank (equation 2.11) and pressure valve opening area at throat 1 (equation 2.3) (see Figure 2.2). The corresponding density (equation 2.10) at throat 1 and valve opening area at throat 1 is also plotted in Figure 2.3.

*Table 2. 2 Summary of the given parameter values of the BSWT*

| Parameter | Description | Value | Unit (SI) |
|---|---|---|---|
| $R$ | Specific gas constant | 287 | Pa m$^3$/(kg K) |
| $\gamma$ | Ratio of specific heats for calorically perfect gas | 1.4 | - |
| $T_T$ | Total temperature at the tank | 294 | K |
| $P_{T_{initial}}$ | Initial total tank pressure | 2.068E6 | Pa |
| $P_P$ | Total pressure in the plenum chamber | 7.929E5 | Pa |
| $V_T$ | Volume of the tank | 5 | m$^3$ |
| $P_{TS}$ | Total pressure in the test section | 7.929E5 | Pa |
| $M_{TS}$ | Mach number in the test section | 2 | - |
| $A_{TS}$ | Cross sectional area in the test section | 0.0103 | m$^2$ |
| point | Evenly spaced points | 1000 | - |
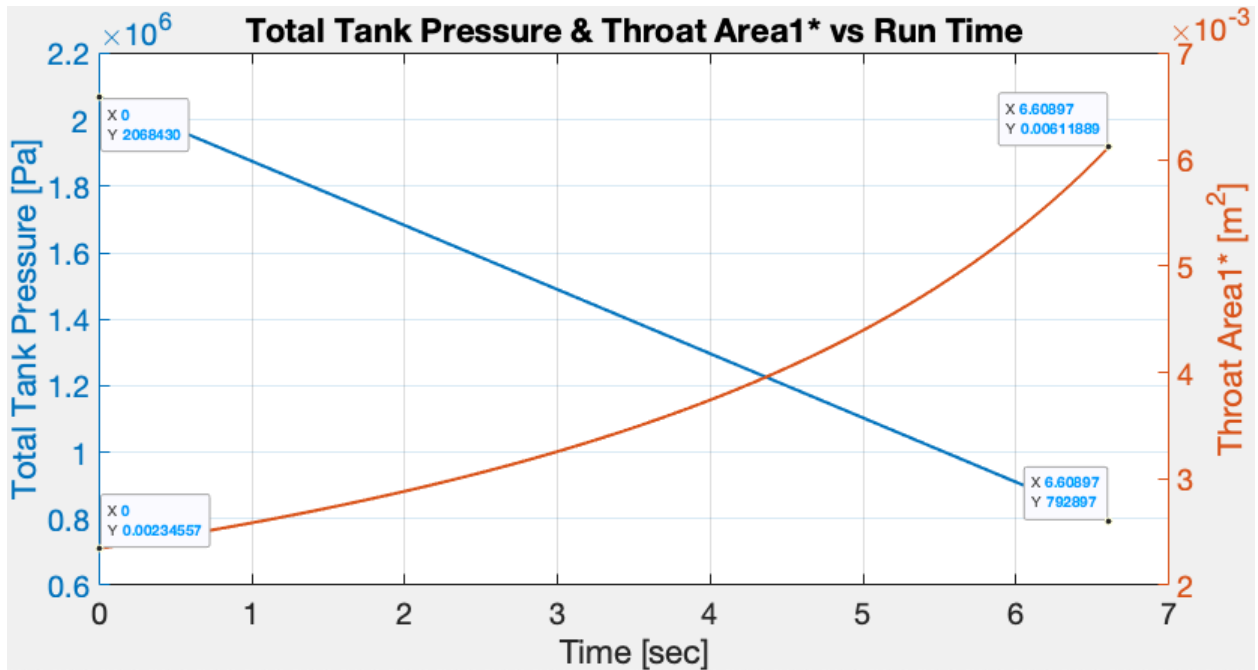
Figure 2. 2 Total pressure in the tank and variable cross-sectional area at throat 1
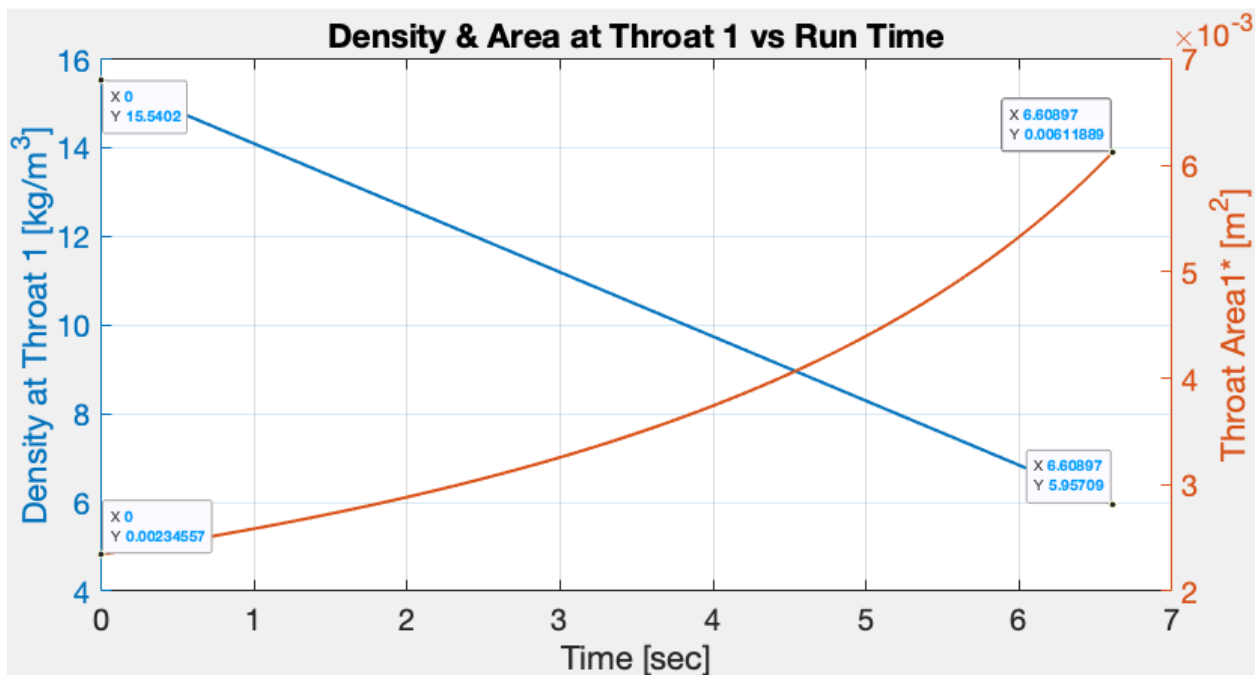


Figure 2. 3 Density and variable cross-sectional area at throat 1

From Figure 2.2, one can visualize that the total test duration of an experiment for a Mach number of 2 in the test section takes about 6.609 s, which is very close to the default time required (about 7 s) of the Fisher valve to become fully open. The valve opening should be set to open to an area of 0.00235 $m^2$ (about 3.6356 $in^2$ ) before the beginning of an experiment. As time progresses, the valve needs to be opened up faster to compensate for the pressure decay in the

tank while maintaining a constant plenum chamber stagnation pressure. At the cutting time of 6.609 s, the valve will be fully opened so the maximum opening area is 0.0061 m$^2$ (about 9.4550 in$^2$). As for the total pressure in the tank, it starts from an initial pressure of 2.068E6 Pa (about 300 psi) at time zero and decreases linearly with run time until reaching the minimum pressure of 7.929E5 Pa (about 115 psi), which is equal to the desired plenum chamber stagnation pressure we like to keep constant. The resulting plots have demonstrated the trends of throat 1 as expected. Figure 2.3 is to show the corresponding density at throat 1. The maximum density happens at time = 0 and is found to be 15.5402 kg/m$^3$.

## 2.2.2 Estimated Solution of the Cross-Sectional Area at Throat 1

In section 2.2.1, the opening area of the valve at throat 1 has been studied analytically. In this section, an estimated solution of the varying cross-sectional area at throat 1 from the valve geometry will be investigated as well to determine the relationship between the analytical solution of $A^*_1(t)$ and the estimated solution of $A^*_{1est}(t)$.

## 2.2.2.1 Flow Path of the Physical Valve

The commercial pressure valve used at SJSU BSWT is called *Fisher$^{TM}$ Vee-Ball$^{TM}$ V300 Rotary Control Valves* with a nominal pipe size (or NPS) of 4 in and ANSI rating of CL300 [24]. The v-notch ball valve rotates to open or close the flow path when the driveshaft it is connected to is turned by an actuator. The range of the turning angle of the shaft is between 0 to 90 degrees. When the valve is set at 0 degrees, the flow path will be blocked. On the other hand, when the valve turns 90 degrees, the passage will be fully exposed. Since the area of the opening passage is the interest of study, three successive cross-sectional profiles are drawn to show the flow path and the v-notch contour in different angles. The images from left to right in Figure 2.4 illustrate how the flow path is revealed through the v-notch as the drive shaft rotates into the paper.
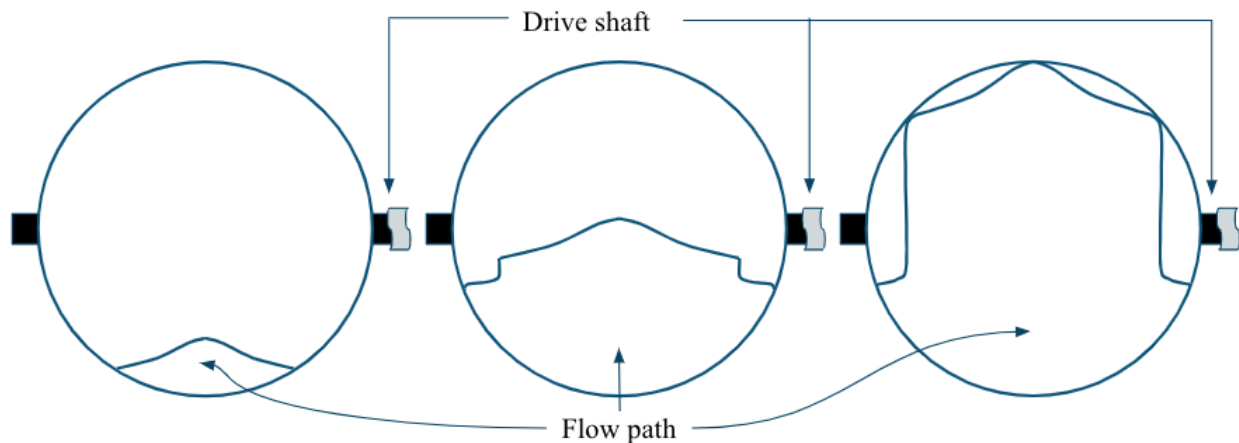


Figure 2. 4 Cross-sectional profiles of the flow path and v-notch ball valve [25]

The contour of the flow path varies depending on the turning angles of the valve. Calculating the cross-sectional area of the flow passage will not be very straightforward due to the complex geometry. Thus, it is necessary to simplify the evolving contours to compute the varying flow area. Keep in mind that a simplified model of the geometry will indeed affect determining the initial valve angle $\theta_{ini}$; when the estimated area is overestimated, the real $\theta_{ini}$

will be underestimated; on the other hand, when the estimated area is underestimated, the real $\theta_{ini}$ will be overestimated.

A simplified method that uses the equation of the overlapping area of two congruent circles is proposed to calculate the area changes as the valve turns at throat 1 [26] as below. Bear in mind that this estimation will oversize the cross-sectional area at throat 1 as one can examine from Figure 2.4.

$$A_{1_{est}}^*(d) = 2R^2 cos^{-1}(\frac{d}{2R}) - \frac{1}{2}d\sqrt{4R^2 - d^2} \qquad (2.14)$$

where R is the radius of the circle, d is the distance between the centers of the two circles. Figure 2.5 is the graphical representation of how the varying overlapping area of two circles is analogous to the varying flow path.
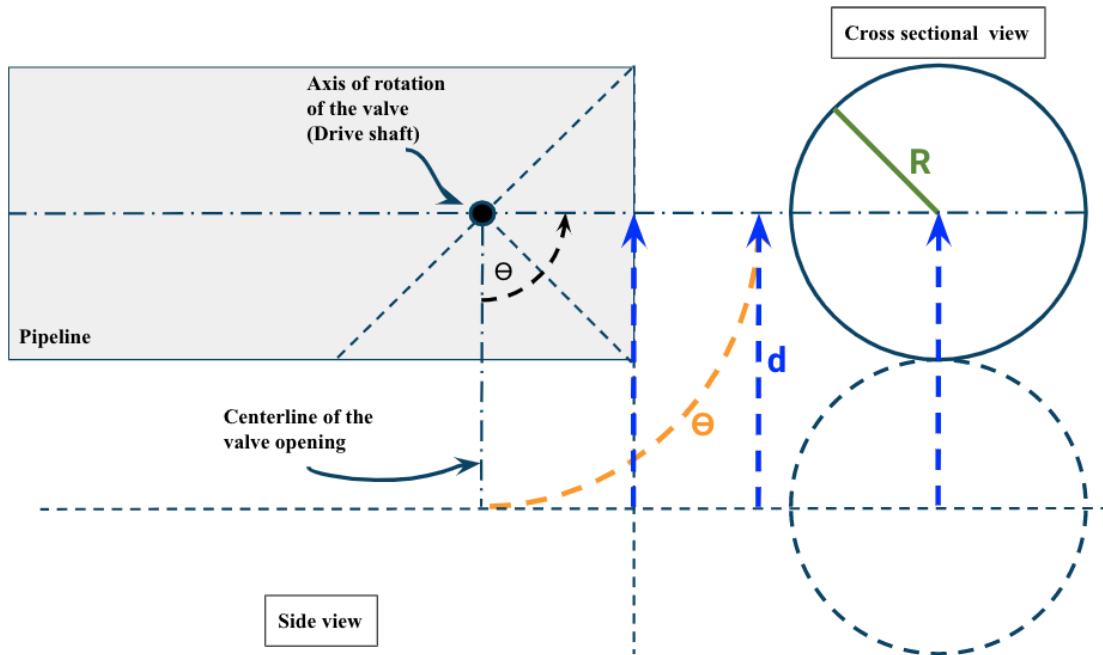


Figure 2. 5 Side view and cross-sectional view of the simplified flow path model

In Figure 2.5, the side view of the pipeline shows the locations of the valve and the drive shaft that turns the valve. The angle of rotation of the valve is denoted as $\theta$ and as aforementioned it spans between 0 ~ 90 degrees. When $\theta$ is set at 0 degrees, the passage of the pipeline will be fully closed. $\theta$ increases as the driveshaft turns counterclockwise until it reaches 90 degrees to fully reveal the flow passage. Examining the cross-sectional view on the right-hand side of Figure 2.5, one can see the two congruent circles conjoint together top and bottom. When the valve turns counterclockwise, one can imagine that the bottom dotted circle moves up which results in some areas overlapping with the top circle. The parameter, d, decreases from its maximum length of 2R, when the tracing of $\theta$ is 0 degree, to its minimum length of 0, when the tracing of $\theta$ is 90 degrees.

Applying trigonometry, the area changing at throat 1 (equation 2.14) can be expressed in terms of $\theta$:

$$A^*_{1_{est}}(\theta) = 2R^2 cos^{-1}(\frac{cos(\theta)d_{max}}{2R}) - \frac{1}{2}cos(\theta)d_{max}\sqrt{4R^2 - (cos(\theta)d_{max})^2} \qquad (2.15)$$

where $d_{max}$ is the maximum distance, which is 2R, between the centers of the two congruent circles.

2.2.2.2 Plot the Valve Opening at Throat 1

Note that the radius of the congruent circles, 0.0441 m, is obtained from backtracking the maximum opening analytical area, which is 0.0061 m$^2$ or 9.4550 in$^2$. With the help of MATLAB, equation (2.15) is plotted as a function $\theta$ (see Figure 2.6).
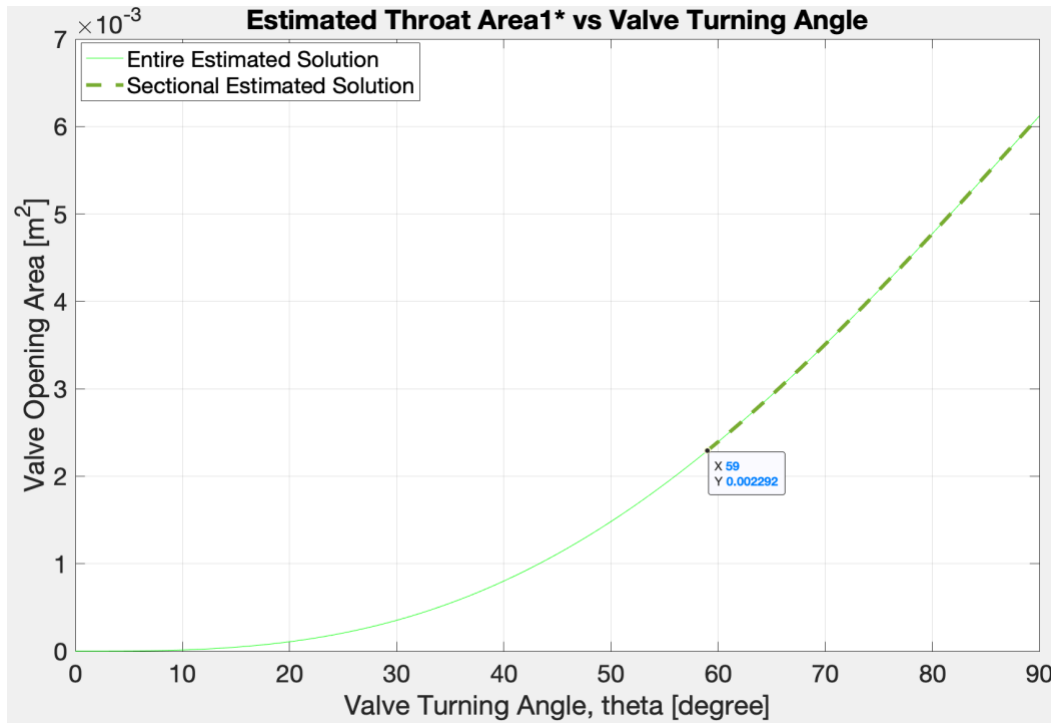


Figure 2. 6 Estimated flow area at throat 1 as a function of $\theta$

## 2.3 Mapping the Estimated Solution to Analytical Solution

The final task is to map the turn angle of the valve to time. From the analytical solution, it is learned that the initial area at throat 1 is not zero. Therefore, the valve should be opened at a certain degree before a run or when run time is equal to zero. Thus, finding this angle at time zero is critical because it serves as the initial point when converting $A^*_{1est}(\theta)$ to $A^*_{1est}(t)$. To obtain this initial angle at time zero, we first extract the later section of the estimated solution by subtracting the minimum analytical area, which is essentially the initial area, obtained in section 2.2.1.4 from the estimated area. Since the angle is discretized, the initial valve angle $\theta_{ini}$ is then

chosen to be the previous angle before the angle that corresponds to the minimum sectional estimated solution.

The later section of the estimated solution is also plotted as the sectional estimated solution in Figure 2.5. From Figure 2.6, the initial value of the valve turning angle is found to be 59 degrees, which corresponds to both the analytical and estimated initial valve opening area of 0.00235 m$^2$ or 3.6356 in$^2$.

The angle-time array $\theta_{time}$ between the determined initial valve turning angle and 90 degrees can be created by using the same number of evenly spaced points as the time array, which is defined as 1000 points in section 2.2.1.2. This one-to-one degree to time mapping indicates that for 1/1000 degrees, the time marching will be 1/1000 seconds. Substituting $\theta_{time}$ for $\theta$ in equation (2.15), the estimated valve opening area at throat 1 becomes:

$$A^*_{1_{est}}(\theta_{time}) = 2R^2 cos^{-1}(\frac{cos(\theta_{time})d_{max}}{2R}) - \frac{1}{2}cos(\theta_{time})d_{max}\sqrt{4R^2 - (cos(\theta_{time})d_{max})^2} \quad (2.16)$$

Table 2.3 summarizes the values given to certain parameters used in equations (2.15) and (2.16) in section 2.3.

*Table 2. 3 Summary of the given parameter values for computing area changing at throat 1*

| Parameter | Description | Value | Unit (SI) |
|---|---|---|---|
| R | Radius of congruent circles | 0.0441 | m |
| d$_{max}$ | Maximum distance between the centers of the two congruent circles | 2R | m |
| $\theta$ | Angle of rotation of the valve | 0~90 | degree |
| $\theta_{time}$ | Angle-time array | $\theta_{ini}$ ~90 | Degree or sec |
| point | Evenly spaced points | 1000 | - |

Figure 2.7 shows the analytical and estimated solutions with respect to time evaluated from equations (2.3) and (2.16) separately. The sectional estimated solution suggests a steadier increase in the rate change of the opening area than the analytical solution. Table 2.4 summarizes the important calculation results from the preliminary analysis of the mathematical modeling of the throat 1 dynamics.
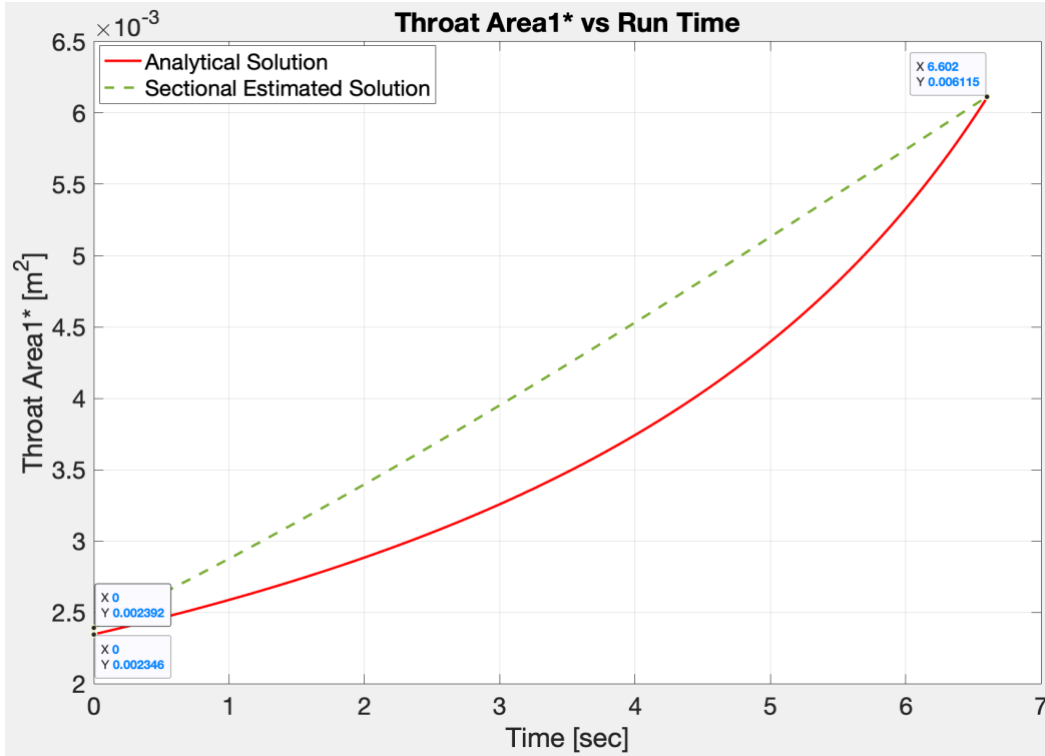
Figure 2. 7 Analytical solution and estimated solution of the area changing at throat 1

*Table 2. 4 Summary of important results from preliminary analysis*

| Parameter | Description | Value | Unit (SI) |
|---|---|---|---|
| duration | Total run time for a test | 6.609 | sec |
| $A_1^*(t=0)$ | Analytical solution of the opening area at time 0 | 0.00235 | $m^2$ |
| $A_1^*(t=6.609)$ | Analytical solution of the opening area at the end of run time | 0.0061 | $m^2$ |
| $\theta_{ini}$ | Initial valve opening angle at time 0 | 59 | Degree |
| $A_{1_{est}}^*(\theta_{time}=0)$ | Estimated solution of the opening area at time 0 | 0.0024 | $m^2$ |
| $A_{1_{est}}^*(\theta_{time}=6.609)$ | Estimated solution of the opening area at the end of run time | 0.0061 | $m^2$ |

  The preliminary analysis results indicate that there is indeed a need for a controller and a valve booster. Rather than applying a PI controller like Braun et al described in paper [2], this paper chooses a PID controller because we want a faster response of the system.

There are several reasons for the use of a PID controller in conjunction with the valve booster. First of all, at time zero or when a test starts, throat 1 needs to have an initial valve opening area of 0.0024 m$^2$ ready for an experiment. Therefore, the implementation of a booster will enable the valve to open swiftly within a second or so for the required flow path at the very beginning of an experiment. Secondly, the curves of the solutions shown in Figure 2.7 indicate that the Fisher v-notch valve needs to open more slowly in the first half of the test and faster after passing half of the run time. The rate change of the cross-sectional area at throat 1 is different along the run time so a PID controller will help manage the variations.

Third, the physical valve has its own valve turning rate, which is different from both the analytical and estimated solutions; if the turning rate of the valve is faster than needed, a controller will help slow down the speed. On the other hand, if the turning rate of the valve cannot react faster enough to catch up to a required rate, a booster will help the valve speed up. Furthermore, both the analytical and estimated solutions of the valve opening areas provide theoretical overviews in ideal situations, which is not true in the real world. For instance, fluid in motion will inevitably generate energy head loss or pressure head loss due to friction in pipes and piping components, such as valves, fittings, etc [27]. Thus, by incorporating a booster and a PID controller in a BSWT, a uniform environment in the test section can be better managed for the fidelity of experiments.

# Chapter 3 - PID Controller of the BSWT

The gist of this chapter is the development of the governing equation that relates the valve opening angle, $\theta$, plenum chamber stagnation pressure, $P_P$, and the PID controller. To begin with, a brief review of PID control theory will be introduced in section 3.1. Also, before diving into the PID controller design pertaining to this project, it is important to differentiate the roles of the variables interested. A controlled variable or the process variable, which is measured by a sensor, is usually the process output of a system. On the other hand, a manipulated variable acts as an actuator and is the product of a controlling mechanism that essentially corrects the difference between the measured and desired controlled variable values. Thus, in the context of the pressure control system, $P_P$ is the controlled variable and $\theta$ is the manipulated variable.

## 3.1 A Brief Introduction of PID Control Theory

The process of a PID control concept with a simple feedback loop is illustrated in Figure 1.4. The actuating error signal is the difference between the desired condition (setpoint) and the condition of the system measured by the sensor. This difference is corrected by the designed PID controller, whose output of the processed information is fed into the plant so that the output signal of the plant will approach the setpoint. If the actuating error signal is zero, which indicates the response of the plant matches the setpoint condition, there will be no corrective action needed from the controller to an actuator. Any disturbances to the plant and noises along the process will be carried down to the error handling unit. The controlled process will repeat when the entire system is in operation.

### 3.1.1 PID Controller

In short, a PID controller, which is known as three modes of control, is an error handling unit [28]. The basic characteristic of a proportional controller, $K_P$, is to directly amplify or reduce the actuating error signal so as to enhance response tracking. While performing the same functionality, an integral controller, $K_I$, is to bring the response closer to the desired set point by summing up all the signals of process outputs over a time period of interest, so it improves the steady-state response. A combination of $K_I$ and $K_P$ controller is able to make a system track the setpoint but there is no control over how fast the system will react. Thus, a system with a faster response can be anticipated by adding a derivative controller $K_D$, which mathematically means the rate of change, to the corrective action. The biggest downside of adding a derivative controller is that it is susceptible to noise.

Extending the block diagram shown in Figure 1.4, the process of the design PID controller on pressure control for the BSWT is illustrated in Figure 3.1.
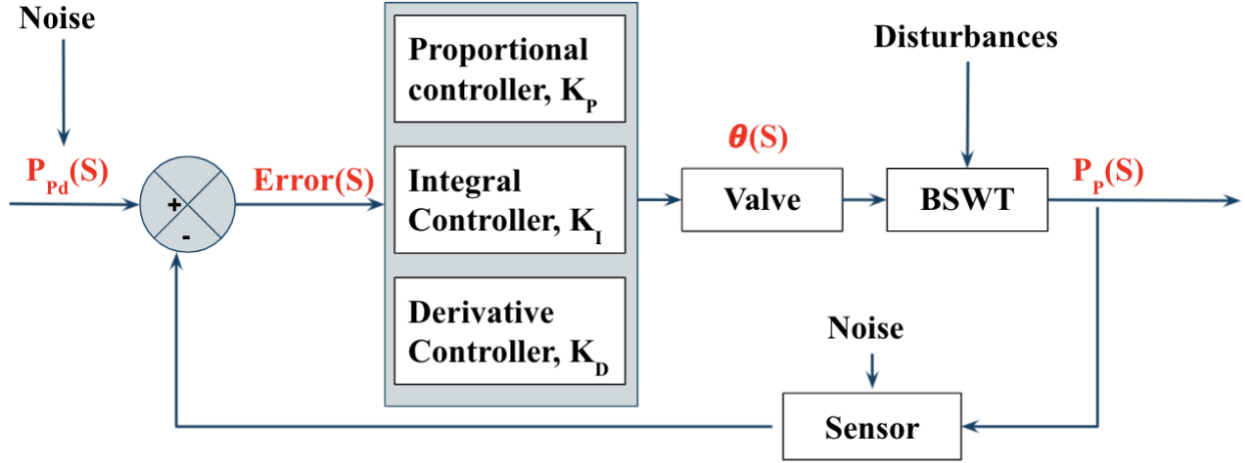
Figure 3. 1 Block diagram of the PID controller for the BSWT in S domain

3.1.2 Transfer Function of a Controller

The relationship between an input and an output of a specific system can be expressed in a transfer function, whose form is written as $\frac{output}{input}$[22]. Thus, in the context of the BSWT, the transfer function, $G_c(s)$, of the PID controller in the complex domain is written as:

$$G_c(s) = \frac{O(s)}{I(s)} = K_P \left(1 + \frac{1}{T_i \, s} + T_d \, s\right) \tag{3.1}$$

where $O(s)$ is the control output, $I(s)$ is the control input, and both $T_i$ and $T_d$ are constant factors applied to the $K_I$ and $K_D$ gains respectively.

Rearrange equation (3.1), $O(s)$ can be expressed as:

$$\begin{aligned} O(s) &= G_c(s)I(s) \\ &= K_P \left(1 + \frac{1}{T_i \, s} + T_d \, s\right) I(s) \end{aligned} \tag{3.2}$$

Depending on the applications, sometimes it is convenient to analyze the control output in the time domain. The control output $O(t)$ in the time domain can be obtained by applying an inverse Laplace transform to equation (3.2).

$$O(t) = K_P I(t) + \frac{K_P}{T_i} \int_0^t I(t) \, dt + K_P T_d \frac{d}{dt} I(t) \tag{3.3}$$

3.1.3 Performance Characteristics

With proper tuning techniques, the gains of the designed PID controller can be obtained to satisfy the performance requirements of a system. The measure of how well the controller is designed is to exanimate the unit-step transient response of the system in the time domain. A

23

unit-step response is often used because it is general enough to represent the response of a system to any inputs [22]. Figure 3.2 is a graphical representation of the performance characteristics.
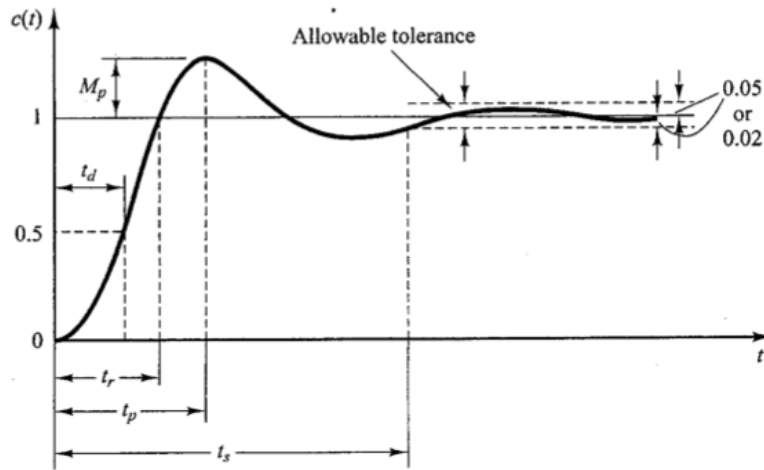


Figure 3. 2 Performance Characteristics of Unit-Step Response [22]

The meaning of the notations in Figure 3.2 is as follow:

- $M_p$: Maximum overshoot
- $t_r$: Rise time
- $t_s$: Settling time
- $t_d$: Delay time
- $t_p$: Peak time

For the PID controller of the BSWT, the metric of performance depends on the types of experiments. For example, a small variation of the Reynolds number (Re) will be accepted if the experiment is about Re transition and will not be for turbulence experiments. Although the controller will be subjected to fine-tune after implementing onto the BSWT, the followings are the desired performance we want to achieve:

- $M_p$: a decent overshoot is desired so as to push the normal shock downstream, but a finite number is to be determined.
- $t_r$: a fast rise time is desired because there is limited time for an experiment, but a finite number is to be determined.
- $t_s$: a fast settling time with 2~3% tolerance is desired because there is limited time for an experiment, but a finite number is to be determined.
- $t_d$: a shorter delay time is desired because there is limited time for an experiment, but a finite number is to be determined.
- $t_p$: a fast peak time is desired because there is limited time for an experiment, but a finite number is to be determined.

24

## 3.2 Governing Equation

Continuing to equation (3.2), the control output $\theta(s)$ can be derived by substituting $\theta(s)$ for O(s) and E(s) for I(s) as shown below. Notice that the actuating error term E(s) is essentially the difference between the desired setpoint $P_{pd}$ and the feedback process output $P_p$.

$$\theta(s) = G_c(s)\, E(s)$$
$$= K_P\left(1 + \frac{1}{T_i\,s} + T_d\,s\right)(P_{Pd} - P_P(s))$$
$$= K_p P_{pd} - K_p P_p(s) + \frac{K_P}{T_i\,s}[P_{pd} - P_p(s)] + K_p T_d\,s\,[P_{pd} - P_p(s)] \tag{3.4}$$

Applying inverse Laplace transform to equation (3.4), $\theta$ becomes:

$$\theta(t) = -K_p P_p(t) + \frac{K_p}{T_i}\int_0^t [P_{pd} - P_p(t))]dt + K_p T_d \frac{d}{dt}[P_{pd} - P_p(t))] \tag{3.5}$$

Taking the derivative of equation (3.5) with respect to time, we have arrived at the governing equation of the valve:

$$\frac{d\theta(t)}{dt} = -K_p \frac{dP_p(t)}{dt} + \frac{K_p}{T_i}[P_{pd} - P_p(t)] + K_p T_d \frac{d^2}{dt^2}[P_{pd} - P_p(t)] \tag{3.6}$$

## 3.3 Numerical Integration Algorithm

The flow process interested in this paper involves four parts: the tank, the pressure valve, the plenum chamber, and the convergent-divergent nozzle at the end of the plenum chamber. From equation (3.6), it is observed that the rate change of the valve angle is essentially dictated by the difference between $P_{Pd}$ and $P_P(t)$ and the rate change of $P_P(t)$. Each derivative term in equation (3.6) will be discretized to obtain the next time step for $\theta(t)$, $P_P(t)$, and the second derivative of $P_P(t)$. The numerical integration begins with i = 1 when time = 0.

During a blowdown test, total pressure from the pressure reservoir will be drained to the plenum chamber through the pressure valve. Thus, we will start by investigating the mass flow rate through throat 1. The mass flow rate through the pressure valve at throat 1 can be determined by the widely used universal gas sizing equation (or volumetric flow rate at standard conditions), which is stemmed from Daniel's Bernoulli's conservation of energy, in the industry [29] [30]:

$$Q_{SCFH} = \sqrt{\frac{520}{GT}} C_G P_T sin\left[\left(\frac{3417}{C_1}\right)\sqrt{\frac{P_T - P_P}{P_T}}\right]_{deg} \tag{3.7}$$

Since the unit in equation (3.7) is in standard cubic feet of air per hour, it needs to be converted into SI units to show the mass flow rate of the valve, $\dot{m}_v$, in kg/s [31]:

$$\dot{m}_v = \frac{2.3741x10^{-8}}{\sqrt{T_T}} C_G P_T sin[(\frac{3417}{C_1})\sqrt{\frac{P_T - P_P}{P_T}}]_{deg} \qquad (3.8)$$

The result of equation (3.8) will be fed forward into the rate changes of $P_T$ and $P_P$ whose updates of time evolution will in return be fed back into $\dot{m}_v$ at the end of each iteration. $\dot{m}_v$ is a function of the valve turning angle $\theta$. The two constants: $C_G$ (gas sizing coefficient) and $C_1$(valve recovery coefficient), are related to the flow coefficient of the valve at rated travel $C_v$:

- $C_G$ relates the critical flow to the absolute inlet pressure to address the problems with predicting critical flow.
- $C_1$ is correction factors addressing the amount of pressure that needs to be recovered from the lowest pressure point slightly downstream of the valve outlet. This coefficient is a function of $\theta$ and can be experimentally determined but is usually provided by the manufacturer of the valve. In general, the range of $C_1$ is between 16 to 37 [30] and sometimes it is derived based on another manufacturer coefficient $X_T$.
- $C_v$ is a function of $\theta$ as well so it can be experimentally determined but is usually provided by the manufacturer of the valve.

Table 3.1 below contains data of $C_v$, $X_T$, which are obtained from the valve manufacturer, $C_1$, and $C_G$ , which are derived from the relationships of $39.76 * \sqrt{X_T}$ and $C_v * C_1$ respectively [32]:

*Table 3. 1 Valve rotation angle vs coefficients for mass flow rate through the pressure valve [33]*

| Valve Rotation Angle [degrees] | 10 | 20 | 30 | 40 | 50 | 60 | 70 | 80 | 90 |
|---|---|---|---|---|---|---|---|---|---|
| $C_v$ | 2.53 | 19.9 | 47.7 | 83.1 | 133 | 186 | 254 | 352 | 534 |
| $X_T$ | 0.776 | 0.658 | 0.642 | 0.614 | 0.530 | 0.493 | 0.440 | 0.354 | 0.240 |
| $C_1$ | 35.0249 | 32.2522 | 31.8577 | 31.1552 | 28.9457 | 27.9171 | 26.3738 | 23.6564 | 19.4783 |
| $C_G$ | 88.61 | 641.82 | 1,519.61 | 2,589.00 | 3,849.780 | 5,192.58 | 6,698.95 | 8,327.04 | 10,401.43 |

Assuming there is no energy loss through the control valve, the rate change of internal energy of the storage tank, is the sum of enthalpy and kinetic energy via the valve [34]:

$$\frac{dU}{dt} = -\dot{m}_v h_v - \frac{1}{2}\dot{m}_v v_v^2 \qquad (3.9)$$

Where $h_v$ is the specific enthalpy of the air going through the control valve and $v_v$ is the velocity of the air going through the control valve.

The rate change of $P_T$ can be approximated by rearranging equation (3.9). $P_T$ is negative because the total pressure in the tank will be depleted during an experiment and $\gamma$ is the ratio of specific heats [2]:

$$\frac{dP_T}{dt} \approx -\frac{\gamma R \dot{m}_v T_T}{V_T} \tag{3.10}$$

Based on the Taylor expansion series, the next time step of $P_{T,i+1}$ can be derived like the following:

$$\begin{aligned} P_{T,i+1} &= P_{T,i} + \Delta t \frac{dP_T}{dt} \\ &= P_{T,i} + \Delta t \left(-\frac{\gamma R \dot{m}_v T_T}{V_T}\right) \end{aligned} \tag{3.11}$$

As for the rate change of $P_P$, mass flow into and out of the plenum chamber must be considered. Similar to the derivation of $P_T$, $P_P$ can be approximated to:

$$\frac{dP_p}{dt} \approx \left[\frac{\gamma R}{V_p}\right][\dot{m}_v T_T - \dot{m}_2^* T_p] \approx \left[\frac{\gamma R T_p}{V_p}\right][\dot{m}_v - \dot{m}_2^*] \tag{3.12}$$

Where $\dot{m}_2^*$ is the mass flow rate through throat 2 and $V_p$ is the volume of the plenum chamber.

$\dot{m}_2^*$ is derived based on the assumptions that the flow is isentropic after the normal shock in the plenum chamber and the flow is choked at throat 2:

$$\dot{m}_2 = \rho_2^* \sqrt{\gamma R T_2^*} A_2^*$$
$$= [\frac{p_2^*}{R T_2^*}] \sqrt{\gamma R T_2^*} A_2^*$$
$$= p_p \frac{p_2^*}{p_p} \sqrt{\frac{\gamma R T_2^*}{R^2 T_2^{*2}}} A_2^*$$
$$= p_p [(1 + \frac{\gamma - 1}{2} M_2^{*2})^{\frac{\gamma}{\gamma-1}}]^{-1} \sqrt{\frac{\gamma}{R T_2^*}} A_2^*$$
$$= [(\frac{\gamma + 1}{2})^{\frac{-\gamma}{\gamma-1}}] \sqrt{\frac{\gamma}{R T_p (\frac{T_2^*}{T_p})}} A_2^* P_p$$
$$= [(\frac{\gamma + 1}{2})^{\frac{-\gamma}{\gamma-1}}] (\frac{T_p}{T_2^*})^{1/2} \sqrt{\frac{\gamma}{R T_p}} A_2^* P_p$$
$$= [(\frac{\gamma + 1}{2})^{\frac{-\gamma}{\gamma-1}}] (1 + \frac{\gamma - 1}{2})^{1/2} \sqrt{\frac{\gamma}{R T_p}} A_2^* P_p$$
$$= [(\frac{\gamma + 1}{2})^{\frac{-(\gamma+1)}{2(\gamma-1)}}] \sqrt{\frac{\gamma}{R T_p}} A_2^* P_p$$

$$(3.13)$$

Similarly, the result of equation (3.12) will be used to update the next time step $P_{P,\,i+1}$ for the first derivative:

$$P_{P,i+1} = P_{P,i} + \Delta t \frac{dP_P}{dt}$$

$$= P_{P,i} + \Delta t [(\frac{\gamma R T_p}{V_p})(\dot{m}_v - \dot{m}_2^*)] \qquad (3.14)$$

Since the step size $\Delta t$ is small ($\leq 0.01$), the second derivative of $P_{p,i+1}$ can be approximated by using any of the finite-difference derivatives on either $P_{p,i+1}$ or $\frac{dP_{p,i}}{dt}$ between two adjacent points. Notice that it is fair to assume that when $i = 1$, the second derivative of $P_p$ is zero:

$$\frac{d^2 P_{p,i+1}}{dt^2} \approx \frac{\Delta^2 P_{p,i+1}}{\Delta t^2} \approx (\frac{dP_{p,i}}{dt} - \frac{dP_{p,i-1}}{dt})\frac{1}{\Delta t} \qquad (3.15)$$

Finally, equation (3.6) can be rewritten in discretized form:

$$\frac{\Delta\theta}{\Delta t} = -K_p \frac{\Delta P_p}{\Delta t} + \frac{K_p}{T_i}[P_{pd} - P_{p,i+1}] + K_p T_d \frac{\Delta^2}{\Delta t^2}[P_{pd} - P_{p,i+1}]$$

$$=> \Delta\theta = -K_p \Delta P_p + \frac{K_p}{T_i}[P_{pd} - P_{p,i+1}]\Delta t + K_p T_d \frac{\Delta^2}{\Delta t^2}[P_{pd} - P_{p,i+1}]\Delta t \quad (3.16)$$

With all the terms computed, the next time step of $\theta$ can be derived to start the next iteration:

$$\theta_{i+1} = \theta_i + \Delta\theta \quad\quad (3.17)$$

# Chapter 4 - Computational Solution of the Process Dynamics

This chapter aims to solve the differential equations developed in chapter 3 to validate the mathematical models of critical elements as well as the entire controlled system by means of computer simulations. To examine if both pressures in the tank and in the plenum chamber will drop as expected, we will turn off the control mechanism, meaning no PID controller and no actuating valve. To mimic the situation, $K_p$, $T_i$, and $T_d$ will be set to 1 and the valve angle $\theta$ will be set to 90 degrees. Later on, once the trends of pressure drops and valve opening angle are checked, a trial set of controller gains obtained from the Simulink PID auto-tuning [35] will be installed to actuate the valve to see the responses of tank pressure and plenum pressure. Moreover, the valve angle where the curve bends will serve as a good indicator to validate the mathematical models; this value should be less than the value found in section 2.3.

The analytical solutions will be solved numerically both by the integration algorithm developed in chapter 3 and by Simulink. The purpose of obtaining the solutions by Simulink is two folds. First is to check if the integration algorithm is implemented correctly because the underlying integration solvers of Simulink are numerical approximation methods too. Second, the Simscape modeling is in the Simulink environment, so the Simulink controller that works exactly the same as the integration algorithm developed can be implemented to test its capability in Simscape modeling of the BSWT later in chapter 5.

A fixed-step size $\Delta t = 0.01$ sec is applied to both approaches. Flow coefficients ($C_1$ and $C_v$) are functions $\theta$. A cubic and a least-squares interpolations are used to map $\theta$ to $C_1$ and $C_v$ respectively[2]. Table 4.1 summarizes the initial values used for $i = 1$ when time $= 0$.

*Table 4. 1 Summary of the initial values used in the numerical algorithm and Simulink*

| Parameter | Description | Value | Unit (SI) |
|-----------|-------------|-------|-----------|
| $C_G$ | gas sizing coefficient | 0 | - |
| $C_1$ | valve recovery coefficient | 39.76 | - |
| $P_{T,i}$ | Initial tank total pressure | 2.0684E6 | Pa |
| $\theta_i$ | Initial valve angle | 0 | degrees |
| $P_{p,i}$ | Initial plenum chamber pressure | 101,325 | Pa |
| $\frac{d^2P_{p,i}}{dt^2}$ | Initial acceleration of plenum chamber pressure | 0 | Pa |

A system of differential equations, namely equations (3.8), (3.10), (3.12), and (3.13), developed in section 3.3 are assembled to compute the time evolutions of $P_T$, $P_p$, and $\theta$. The solutions are computed by both the numerical algorithm in Matlab and the Simulink and are described in sections 4.1 and 4.2 separately. A short discussion will be followed in section 4.3.

## 4.1 Solution from Numerical Algorithm

Figure 4.1 shows the solutions of tank pressure, plenum chamber pressure, and valve angle without the implementation of a PID controller. From this figure, it can be observed that as soon as the valve opens from $0^o$ at time zero to $90^o$, the tank pressure starts dropping and the

plenum chamber pressure rises from its initial ambient pressure to equilibrium condition due to the high-pressure influx from the tank within around 0.13s. Both tank pressure and settling chamber pressure drop together until both reach ambient pressure.

Figure 4.2 depicts the solutions when a PID controller is implemented. The PID gains used here are obtained from the PID Tuner feature in the PID Controller block from Simulink just to roughly gain some insight about how the system responds to valve opening angle but they have not been optimized yet. It is observed that, with Kp = 9.9602E-6, Ti = 0.0199, and Td = 0.00498, the plenum chamber pressure is able to be maintained at a constant level for a period of time when the valve is controlled.
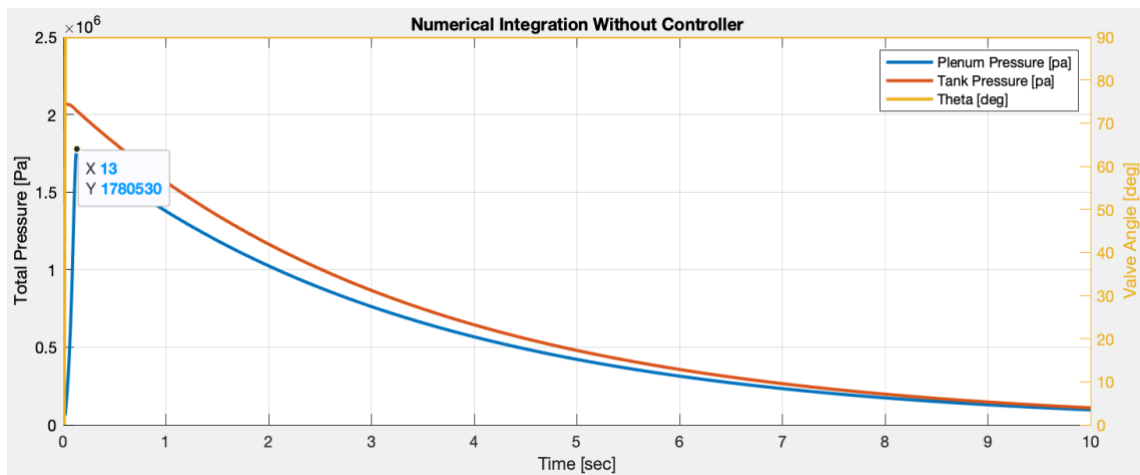


Figure 4. 1 Solutions without a controller computed by a numerical algorithm
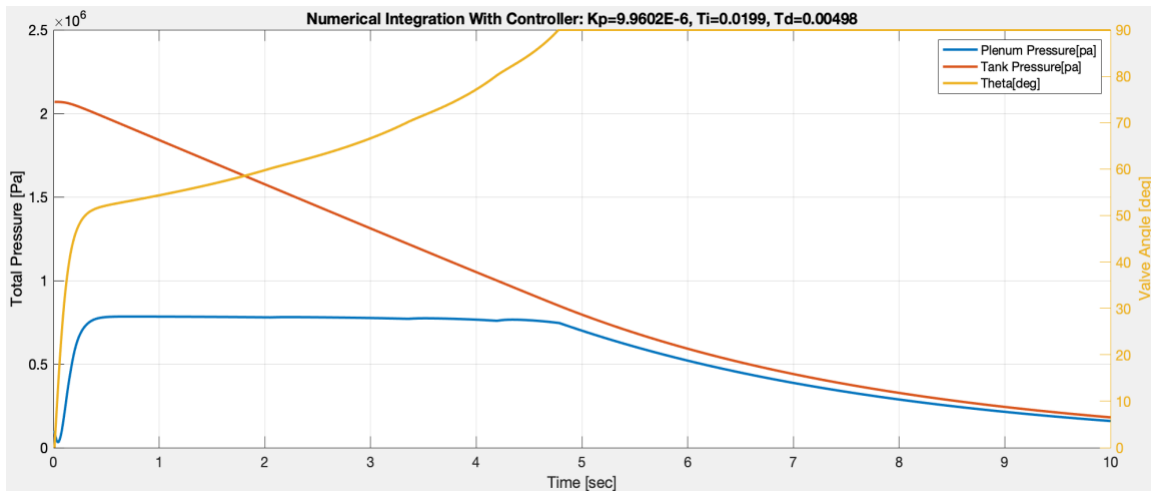


Figure 4. 2 Solutions with a PID controller computed by a numerical algorithm

31

## 4.2 Solution from Simulink

Another way to numerically solve the system of equations is to use Simulink. Note that the default numerical integration solver in Simulink is an auto solver, which may or may not be a fixed-step solver. Since the result will be used to validate the numerical algorithm, we will specifically set the type to be a fixed-step solver. Figures 4.3 ~ Figure 4.6 are Simulink block diagrams representing the model of pressure-controlled BSWT.

Block diagrams in Figure 4.3 represent the entire pressure-controlled BSWT. The summing junction takes in both the desired plenum chamber pressure as well as the sensing feedback of plenum chamber pressure and outputs the pressure difference. The pressure difference is then handled by the PID controller to find the valve turning angle needed to track the desired plenum chamber pressure (Figure 4.4). Note that the if-else blocks between the angle theta saturation and the valve angle are merely a feature added into the PID controller subsystem block to convenience the user when executing the script from the Matlab console. Thus, they do not affect the control scheme at all.

By using a lookup table (LUT) based on Table 3.1 in chapter 3, the corresponding flow coefficients $C_1$ and $C_v$ to the valve turning angle are generated (Figure 4.5). Together with those coefficients, constants such as TO, R, VOL_TK, VOL_PL, GAMMA, and a2Star are fed into the system of differential equations (mainly equations 3.8, 3.10, 3.12, and 3.13) to solve for the plenum chamber pressure, which is shown in Figure 4.6. Finally, the resulting plenum chamber pressure is feedback to the summing junction to prepare for the next iteration.
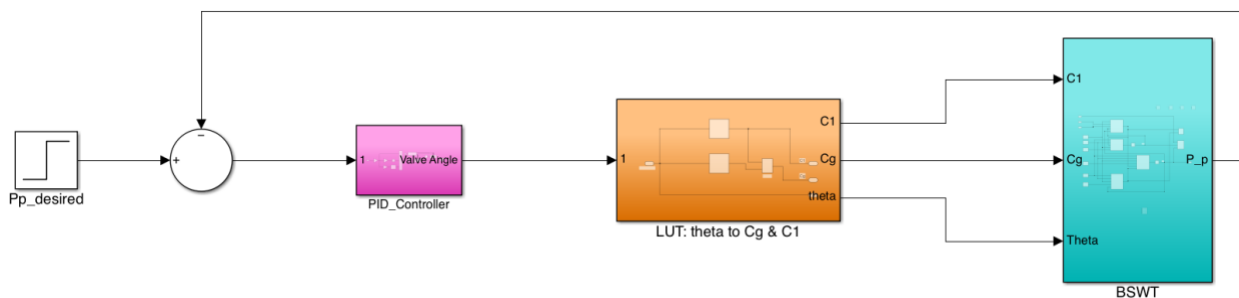


Figure 4. 3 Block diagram: pressure-controlled BSWT
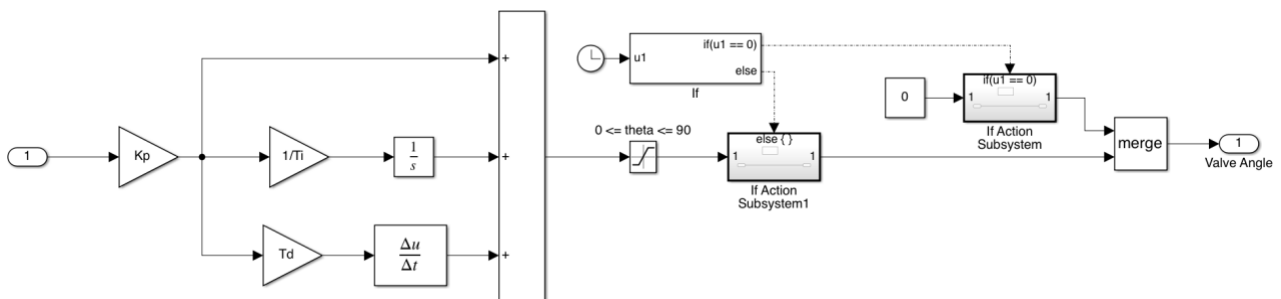


Figure 4. 4 Block diagram: Inside view of PID controller subsystem block
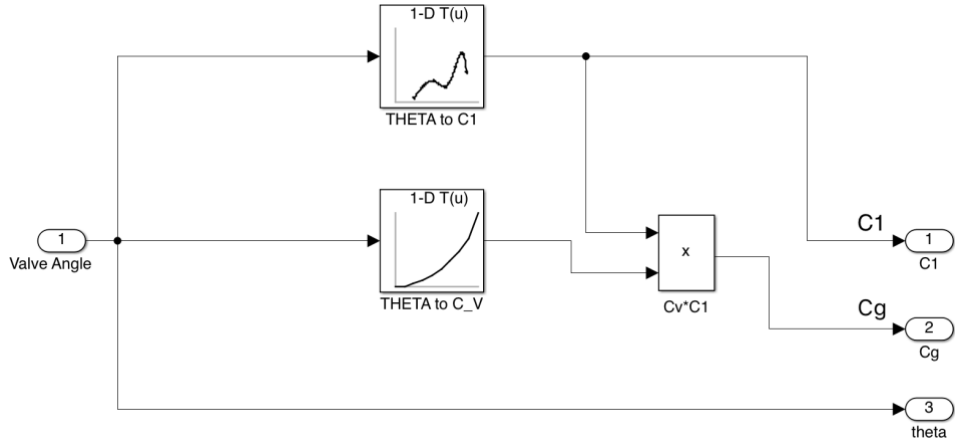
Figure 4. 5 Block diagram: Inside view of LUT subsystem block
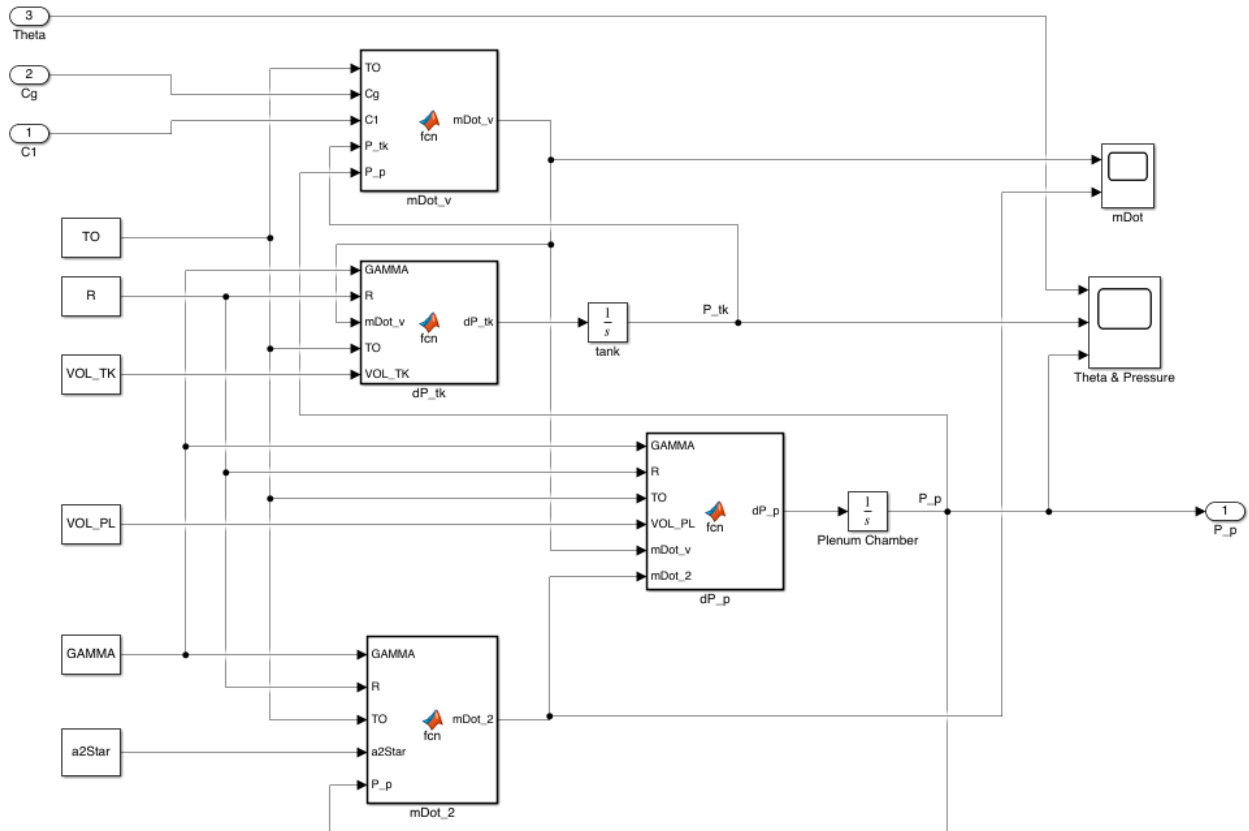


Figure 4. 6 Block diagram: Inside view of BSWT subsystem block

Solutions without and with a PID controller generated from the Simulink Ode1be fixed-step solver, whose step size is 0.01 sec, are presented in Figures 4.7 and 4.8 respectively. In Figure 4.7, it is shown that when there is no control mechanism in place, tank pressure drops and plenum chamber pressure rises from their initial conditions as soon as the valve turns from 0º at time zero to 90º. Eventually, both pressures decrease to ambient pressure as the tank pressure is been depleted.

Figure 4.8 shows the responses of the tank and settling chamber pressures as the valve is under control by the same PID gains used to generate the results from the numerical algorithm, which is shown in the previous section. When the valve is regulated by the PID controller, the plenum chamber pressure can be kept at a constant level for a certain duration.
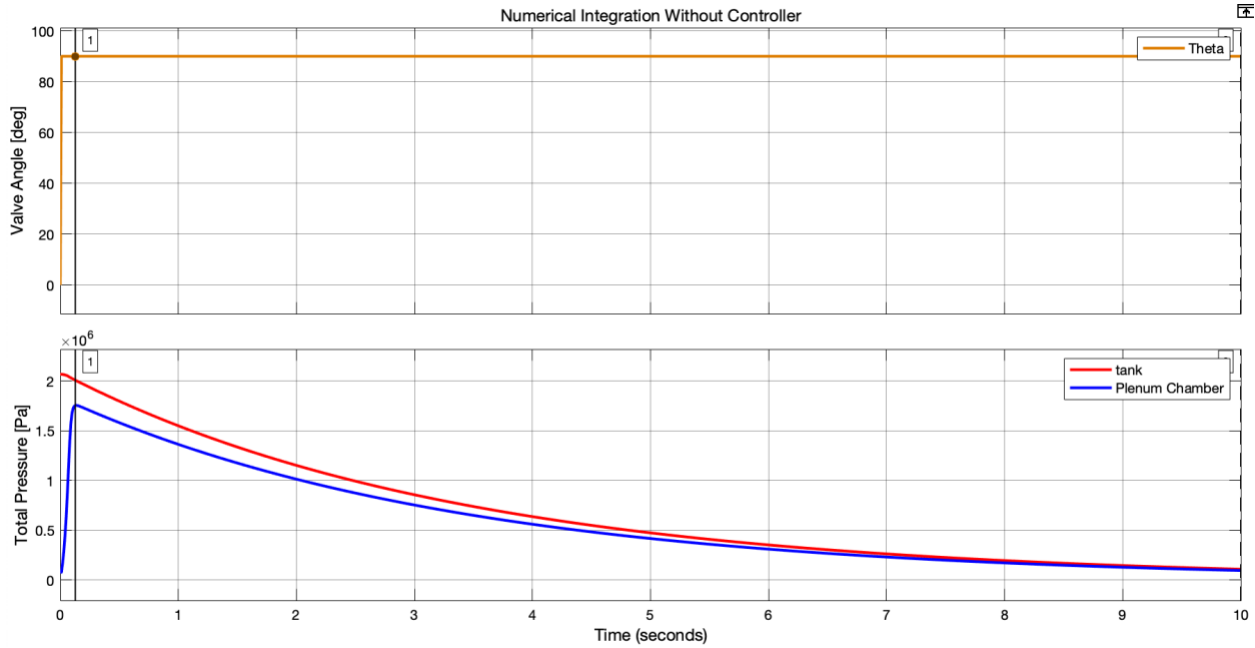

Figure 4. 7 Solutions without a controller computed by Simulink
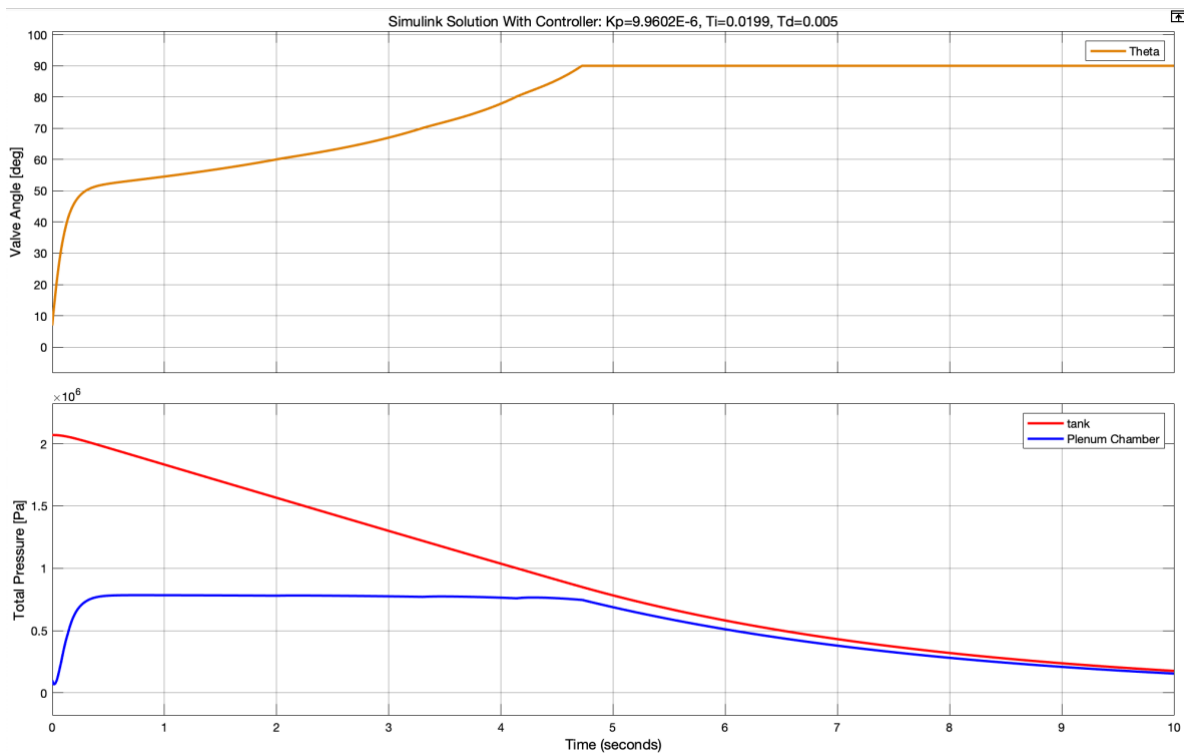

Figure 4. 8 Solutions with a PID controller computed by Simulink

## 4.3 Discussion

From Figure 4.1 and 4.7, it is observed that without the implementation of a PID controller, the time evolutions of $P_T$, $P_p$, and $\theta$ found from both the numerical algorithms and Simulink are the same. $P_T$ drops progressively. $P_p$ rises from the atmospheric pressure, trying to catch up with $P_T$ immediately after the valve is fully opened and quickly drops along with $P_p$ afterward.

With the installation of a PID controller, the valve that works as an actuator is able to maintain constant $P_p$ with a controlled angle $\theta$ dictated by the controller. The responses of $P_T$ and $P_p$ can be seen in Figures 4.2 and 4.8. Again, the results from both the numerical algorithms and Simulink are the same. $P_T$ drops slightly slower than without a controller while $P_p$ rises until the moment where the valve angle reaches the corner value (the first bend of the $\theta$ curve) and drops right after $\theta$ turns to its maximum of 90 degrees (the second bend of the $\theta$ curve).

Another information that can be distilled from the result when a controller is in place is the settling valve opening angle for maintaining constant $P_p$. From section 2.2.1 we know that the valve must be swiftly opened to compensate for the drastic pressure difference between the tank and the plenum chamber promptly after an experiment starts. In section 2.2.2, the estimated settling valve opening angle is found to be 59 degrees to keep the desired $P_p$. However, we know that the cross-sectional profile of the flow path in throat 1 is oversized in that estimation model. That means the real physical valve should have that settling valve opening angle below 59 degrees when there is no $P_p$ overshoot. This expectation is indeed satisfied by examining the result plots in Figure 4.9. In Figure 4.9, the settling valve opening angle is found to be around 51.64 degrees with the set of PID gains used in Simulink, which is well below 59 degrees. Note that, with different sets of PID controller gains, this settling valve opening angle may vary but they should all be below the threshold value of 59 degrees.
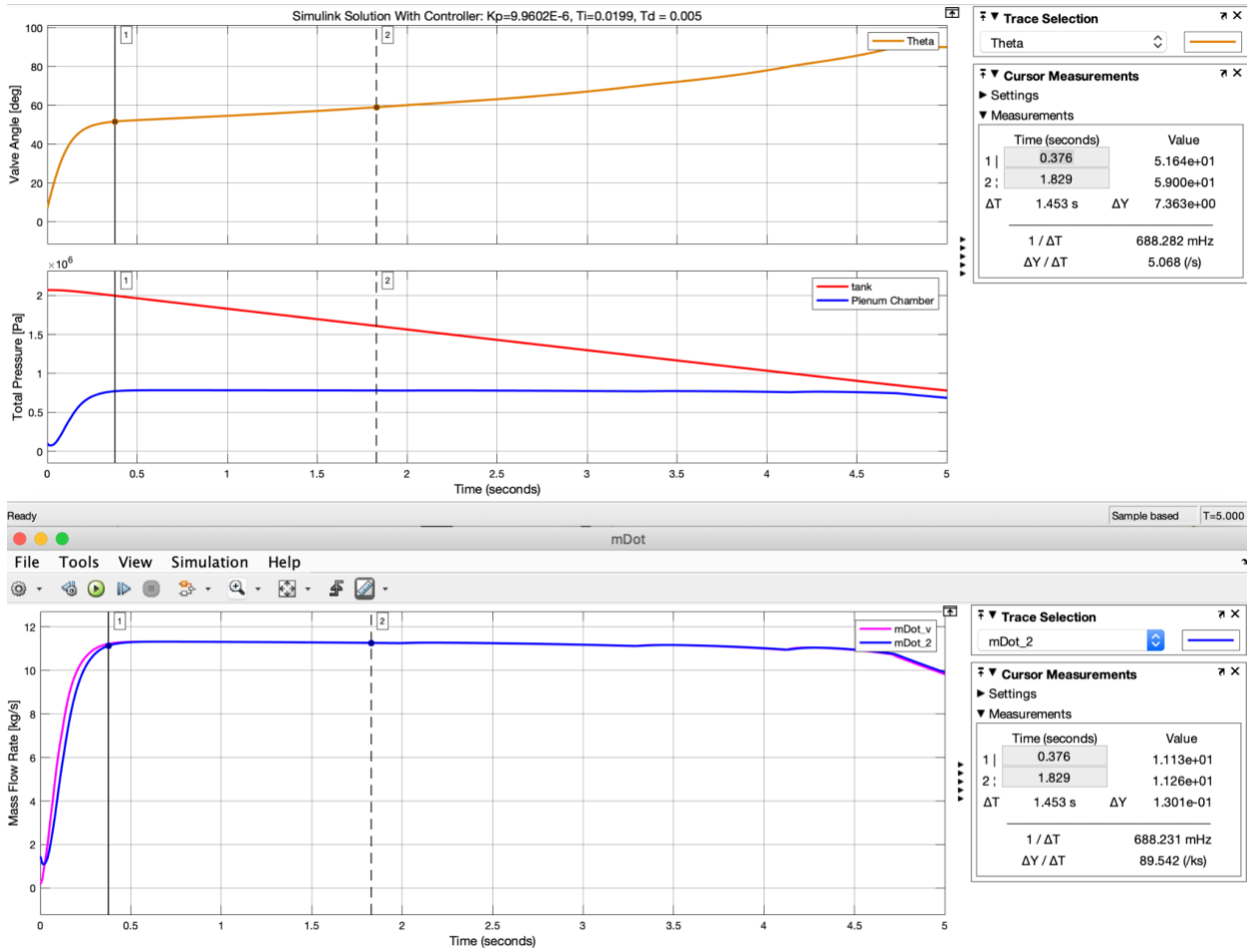
Figure 4. 9 Values of $\theta$, $P_T$, $P_p$, and $\dot{m}$ from Simulink

# Chapter 5 - Simscape BSWT Modeling

This chapter will describe how the physical BSWT is modeled by using Simscape Fluids in conjunction with the Simulink toolbox in the Simulink environment [36] to mimic hardware in the loop (HIL) testing of the PID controller. In general, the physical gas dynamics are captured in the Simscape domain. The physical signals of sensor readings of the plenum chamber pressure and tank pressure from the Simscape domain will be converted to signals that the Simulink controller can read to handle the actuating error. Notice that, with the absence of a rotary ball valve in the Simscape library, there is no angle measurement feedback to the controller system. Instead, the corresponding valve turning angle is transformed to valve cross-sectional area and converted back to Simscape physical signal to actuate the pressure valve in the Simscape domain.

Choosing the right Simscape and Simulink solvers is critical for a successful physical simulation. For the global Simulink solvers, a variable-step solver called *daessc* is selected from the Simulink Model Settings as shown in Figure 5.1. Figure 5.2 is the overview of the entire system constructed by the Simscape blocks and Simulink controller in the Simulink environment.
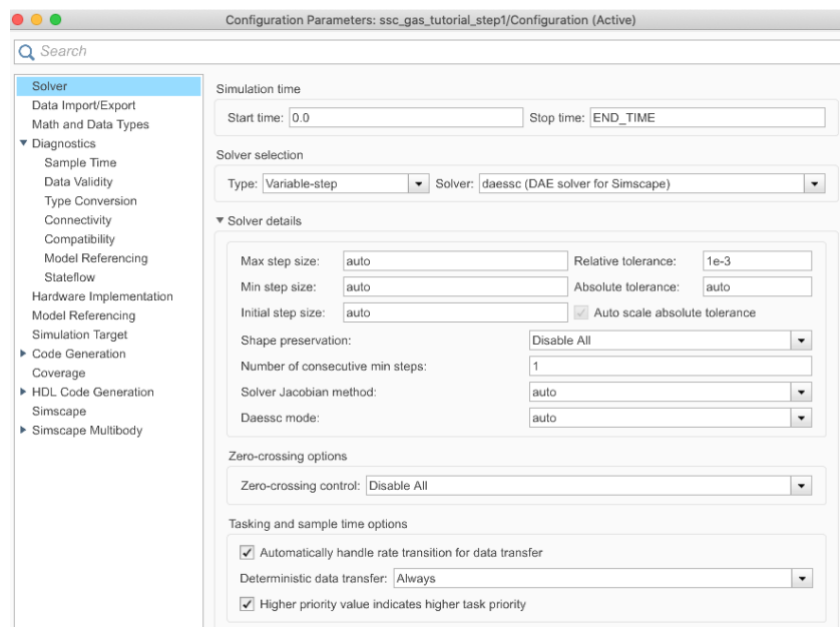


Figure 5. 1 Global solver configuration

Figure 5. 2 BSWT model in Simulink environment

After the Simscape modeling is constructed, the control mechanism will be turned off to examine if the tank and plenum chamber pressures drop as expected by setting $K_p$, $T_i$, and $T_d$ to 1 and valve angle $\theta$ to 90 degrees respectively. The parameters of component geometry are taken from the real design (see appendix A and appendix B) that will be used to construct the tunnel at the time when this report is generated, and the values of the variables representing those parameters are passed from the Matlab script (see appendix C).

# 5.1 Simscape BSWT Model Network

In the absence of a real BSWT plant, the essential components such as pressure tank, sectional gas piping, rotary ball valve, settling chamber, test section, and the diffuser will be modeled by using the Simscape tooling blocks. Note that some of the elementary tooling blocks provided in Simscape libraries do not fully represent the components needed in modeling the plant. So, some of the elementary blocks will be modified to capture the component physics. The following subsections will describe the essential components used in building the gas network of BSWT.

## 5.1.1 Pressure Tank

Since there is no pressure tank element in Simscape modeling libraries, One-Inlet Tank (G-TL) block is used as an alternative (Figure 5.3). Settings of the parameters and Variables are shown in Figure 5.4 and Figure 5.5.
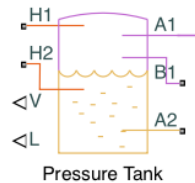


Figure 5. 3 Simscape block: One-Inlet Tank (G-TL)



Figure 5. 4 Settings of pressure tank: Parameters settings
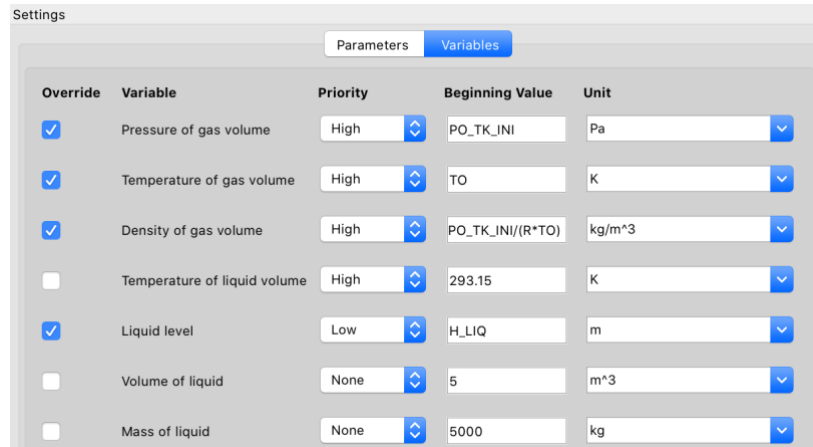
Figure 5. 5 Settings of pressure tank: Variables settings

By default, this block is designed to pressurize the liquid by increasing the gas volume in the tank. A work around to turn this component into a compressed gas tank is to keep the liquid in the tank at a constant low level and drain the gas through port A1 only when the control valve is opened. By default, the total tank volume is made up of unmixed gas and liquid volumes. Notice that since there is no gas gate valve in the Simscape libraries, the air in the sectional piping that directly joins the tank (refer the Appendix A) is treated as a part of the total compressed gas needed, which is 5 m$^3$, in the simulating plant. Therefore, the total tank volume is the sum of the gas and liquid volume in the tank minus the gas volume in the sectional piping. Another important setting is in the variables section; the priorities of initial pressure, initial temperature, and initial density of gas volume need to be set high so when there are conflicts with other variables, the parameters with high priority will become dominated over the variable with low priority [37].

## 5.1.2 Sectional Gas Piping

High-pressure flow inside the gas tank and this sectional gas piping travels to the settling chamber through the control valve and this sectional gas piping is modeled by a Pipe (G) block. Once again, since there is no gas gate valve in the Simscape libraries, the conduit between the pipe gate valve and the control valve shown in Appendix A is neglected in the Simscape model of the BSWT. The flow dynamics network of the pipe is constructed as shown in Figure 5.6. In general, the pipe block is used to model the pipe flow dynamics that account for viscous friction losses and convective heat transfer with the pipe wall. Thus, the heat transfer of the pipe wall via convection is modeled by joining the H port to a Convective Heat Transfer block so that the heat is released to the atmosphere. Since a pipe has a finite volume of gas, the state of the gas volume needs to be declared as the initial condition so that the block is not seen as void space when the high-pressure gas flows into part A at the beginning of the simulation. By default, the variables of standard pressure, which is 0.101325 MPa, and temperature, which is 295.15 K, of gas volume have high priority [38]. However, as aforementioned, the volume of the high-pressure air in this piping is a part of the compressed air needed for the experiment. Therefore, the initial pressure and temperature of the gas volume is the same as the conditions in the tank.
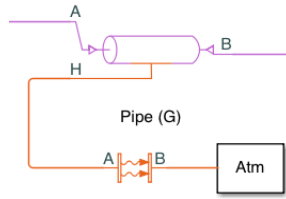
Figure 5. 6 Simscape block: Pipe (G), Convective Heat Transfer, and Atm

  Figures 5.7 and 5.8 are the geometry and variables of the pipe. For supersonic flow, since the inertial force will be dominant over the viscous force, the boundary layer will mostly be made out of the turbulent flow. For this reason, the default values of the laminar flow upper Reynolds number limit and Turbulent flow lower Reynolds number limit as shown in Figure 5.9 are applied catch the phenomenon of flow transition [38].



Figure 5. 7 Settings of pipe: The geometry



Figure 5. 8 Settings of pipe: The initial state of the gas volume



Figure 5. 9 Settings of pipe: Friction and heat transfer of the element

## 5.1.3 Valve

　　The BSWT at SJSU uses the Fisher rotary ball valve to regulate pressure. However, since there is no rotary ball valve block in Simscape libraries, a Local Restriction (G) element is used to model the cross-sectional area of the valve (Figure 5.10). The pressure gas flows through the valve, whose cross-sectional throat area is controlled by the AR signal from the Simulink PID controller, from port A and to port B. The settings of the valve are shown in Figure 5.11. The source of the AR signal is discussed in section 5.2.
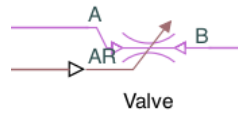


Figure 5. 10 Simscape block: Local Restriction (G)



Figure 5. 11 Settings of valve

## 5.1.4 Settling Chamber

　　The settling chamber is modeled by using a Pipe (G) block because there is no gas chamber element in Simscape libraries. Figure 5.12 shows how the gas coming out from the valve enters and leaves the setting chamber from port A to port B. The settings of the chamber geometry is shown in Figure 5.13. The friction and heat transfer is the same as the sectional piping that connects the tank and the valve. As for the initial state of the gas volume, the priority is given to the pressure and density as shown in Figure 5.14.
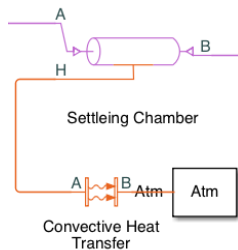


Figure 5. 12 Simscape block: Pipe (G), Convective Heat Transfer, and Atm
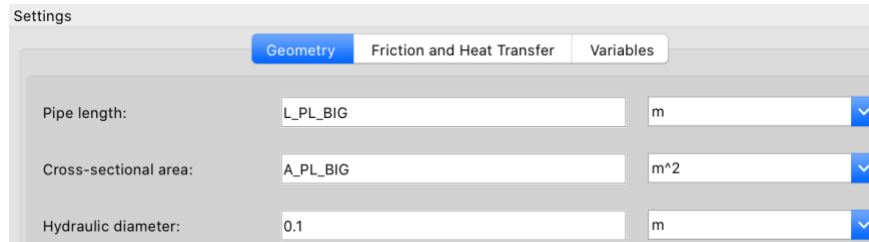
Figure 5. 13 Settings of settling chamber: Geometry
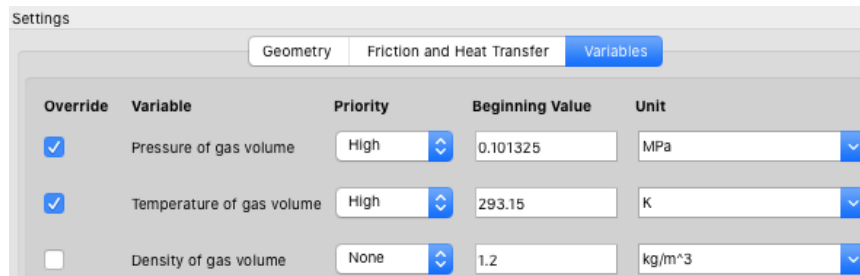


Figure 5. 14 Settings of settling chamber: The initial state of the gas volume

## 5.1.5 Throat 2

Throat 2 between the settling chamber and the test section is modeled by a fixed type of Local Restriction (G) block, which is shown in Figure 5.15. This block is the same one used in modeling the valve. The difference is that a fixed type is chosen in the parameters settings as depicted in Figure 5.16.
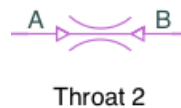


Figure 5. 15 Simscape block: Local Restriction (G)
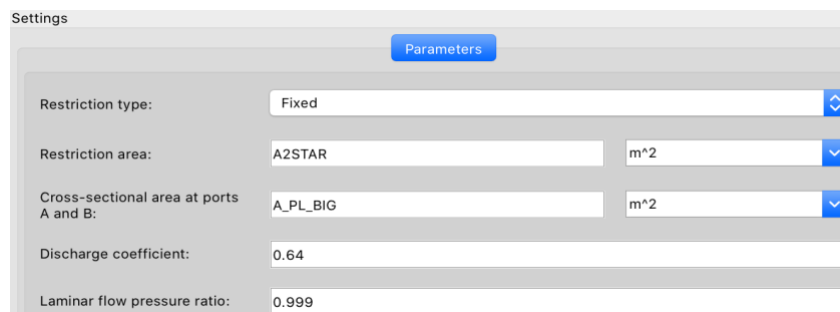


Figure 5. 16 Settings of throat 2

43

## 5.1.6 Test Section

Similar to the settling chamber, a Pipe block is modified to represent the test section. Likewise, the heat convection is joined via port H as shown in Figure 5.17. The test section geometry is pictured in Figure 5.18. The settings of the friction and heat transfer as well as the variables are the same as the settling chamber, so the screenshots of the settings are neglected here.
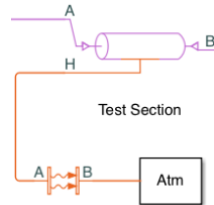


Figure 5. 17 Simscape block: Pipe (G), Convective Heat Transfer, and Atm
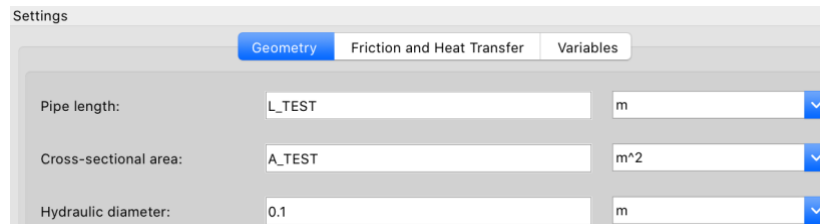


Figure 5. 18 Settings of the test section

## 5.1.7 Throat 3 of Diffuser

Flow after the test section continues traveling to the diffuser part through a constant duct of throat 3 to decelerate the supersonic flow to subsonic speed. Like the Pipe sub-system gas network, the constant throat 3 after the test section is modeled as depicted in Figure 5.19. Since the effects of viscous force play an equally important role as the inertial force in subsonic condition, two flow parameters, namely the Laminar flow upper Reynolds number and the Turbulent flow lower Reynolds number limits, in the friction and heat transfer tab need to be modified to address the effects (refer to Figure 5.20). Thus, a conventional Renolds number range will be applied to account for the flow transition inside the boundary layer [1]. The geometry of the diffuser throat is described in Figure 5.21. As for the initial state of the gas volume, standard pressure and temperature are used to describe the initial states of the flow like the settling chamber.
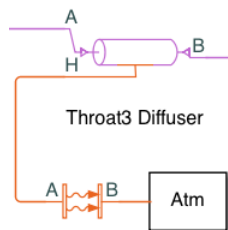


Figure 5. 19 Simscape block: Pipe (G), Convective Heat Transfer, and Atm

44
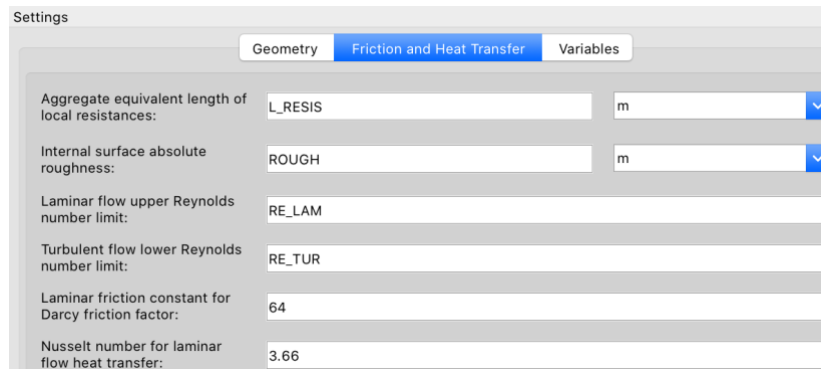
Figure 5. 20 Settings of throat 3: Friction and Heater Transfer
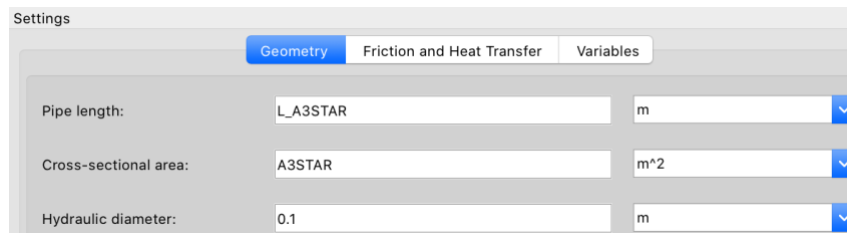


Figure 5. 21 Settings of throat 3: Geometry

## 5.1.8 Diffuser

After the constant duct of throat 3, flow leaves the BSWT from the divergent part of the diffuser to the atmosphere. The sub-system gas network of the diffuser is depicted in Figure 5.22. Except for the geometry settings, which is shown in Figure 5.23, the rest of the parameter values used are the same as those in the constant duct of throat 3 so screenshots of the settings are neglected here.
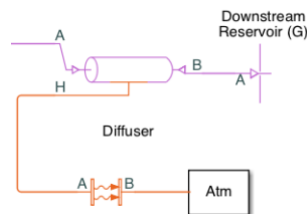


Figure 5. 22 Simscape block: Pipe (G), Convective Heat Transfer, and Atm
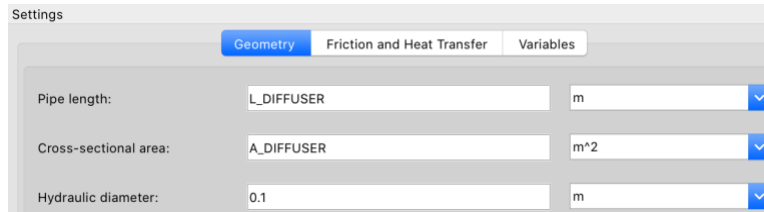
Figure 5. 23 Settings of diffuser geometry

## 5.1.9 Pressure Sensor

The tank pressure and plenum chamber pressure are measured with respect to absolute 0 references by a Pressure & Temperature Sensor (G) block in the gas library. As shown in Figure 5.24, the measurements of tank pressure and settling chamber pressure are converted to P_tk and P_p signals respectively that Simulink can read from port P through a PS-Simulink Converter element.
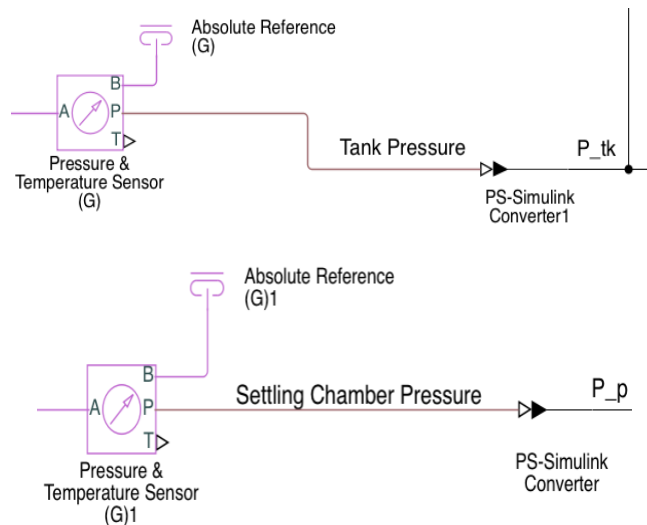


Figure 5. 24 Simscape block: Pressure & Temperature Sensor (G), Absolute Reference (G), and PS-Simulink Converter

## 5.2 Simulink Controller Block

As described in section 5.1.9, the tank and plenum chamber pressure measurements are converted to P_tk and P_p signals so that the actuating error can be corrected by the design PID controller in Simulink. The required cross-sectional throat area then is output to the Simscape domain via a Simulink-PS converter block as shown in Figure 5.25. An expansion view of the Simulink Controller block is shown in Figure 5.26. In general, the control process, elements inside the PID_controller as well as the LUT Theta to Cg & C1, and the network design here are the same as those described in chapter 4.2.

46
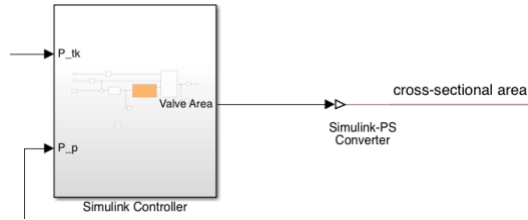
Figure 5. 25 Connection to Simulink Controller block
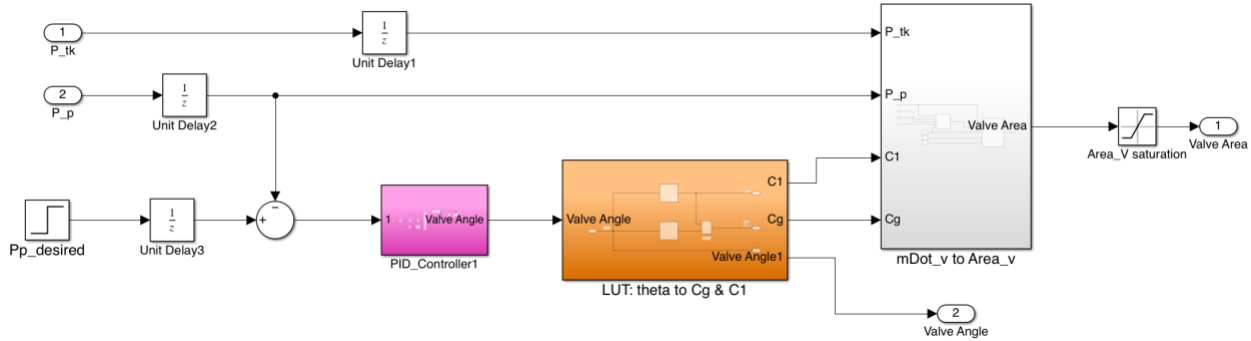


Figure 5. 26 Expansion view of Simulink Controller block

Different from Figure 4.3, there are two modifications made to the pressure controller as shown in Figure 5.21. The first one is the addition of two Unit Delay blocks after the measurements of the tank and plenum chamber pressures and one Unit Delay block after the desired plenum chamber pressure set point. Because the PID controller action is prioritized in the Simscape modeling process at the beginning, those unit delays are introduced to inject the initial data to the PID controller for one sample period in the first iteration; the measurement signals and the desired plenum chamber pressure will be read in from the second iteration of the process. The initial data in those unit delay blocks for the tank pressure, plenum chamber pressure, and the desired plenum chamber pressure are $P_{T,i}$, $P_{P,i}$, and $P_{P,i}$ respectively. Therefore, when the simulation starts, there is no pressure error for the controller to correct.

The second modification is the subsystem joined after the "LUT: theta to Cg & C1 subsystem" as shown in Figure 5.27. Ideally, the controller structure should be built around the valve angle theta increment (equation 3.16) and take in the real-time measurements of tank pressure, plenum chamber pressure, and valve angle from a data acquisition system as described by Braun et al.[2] for SJSU's BSWT. However, due to the lack of rotary ball valve block from the Simscape libraries as mentioned previously, the manipulated control variable is total valve area instead, which is computed by using equation (2.3). Notice that this modification may result in a rapid change of the valve angle, which might become impossible to realize by a real valve actuator, in the transient period.

The actuating signal of the valve area is computed by the mass flow rate at the valve (equation 3.8), which is obtained by the measured pressure signals (P_tk and P_p), the control flow coefficients (C1 and Cg), and constant temperature (TO), as well as the other constant values (TO, GAMMA, and $R$) as shown in the block expansion view in Figure 5.21.

47
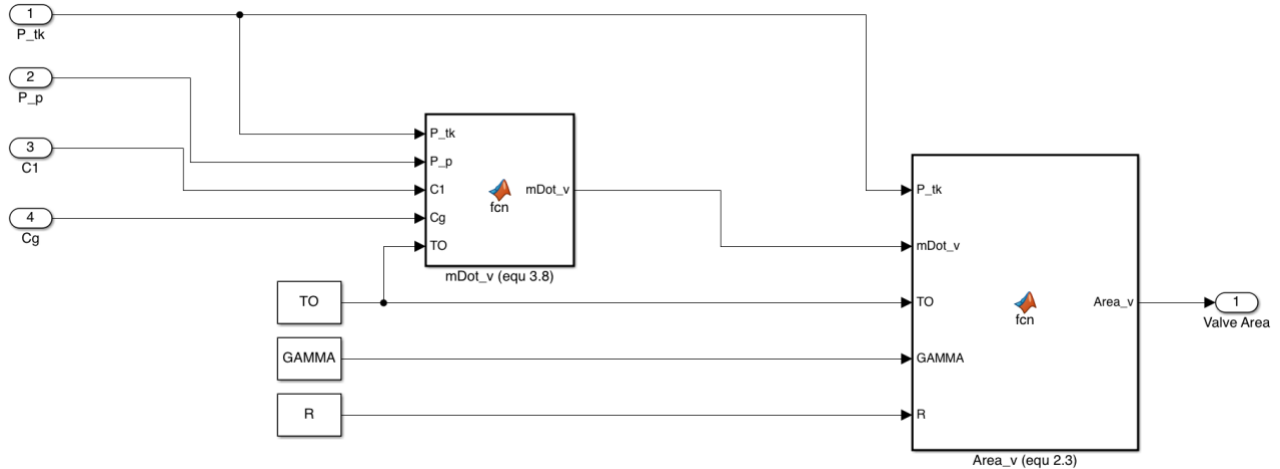
Figure 5. 27 Expansion view of mDot_ to Area_v block

## 5.3 Close-Loop System Response

Similar to chapter 4, the tank and plenum chamber pressures drop will be first checked to see the closed-loop system response without the implementation of the pressure controller, which can be achieved by setting $K_p$, $T_i$, and $T_d$ to 1 and valve angle $\theta$ to 90 degrees respectively. As shown in Figure 5.28, the plenum chamber pressure exhibits organ piping as described in paper [2] after the swift opening of the valve. Also, due to a finite filling time, the plenum chamber pressure does not reach an equilibrium point as fast as the numerical simulation, which reflects a real-world situation. Without any control mechanism, the plenum chamber pressure rises and decreases freely along with the venting of tank pressure.
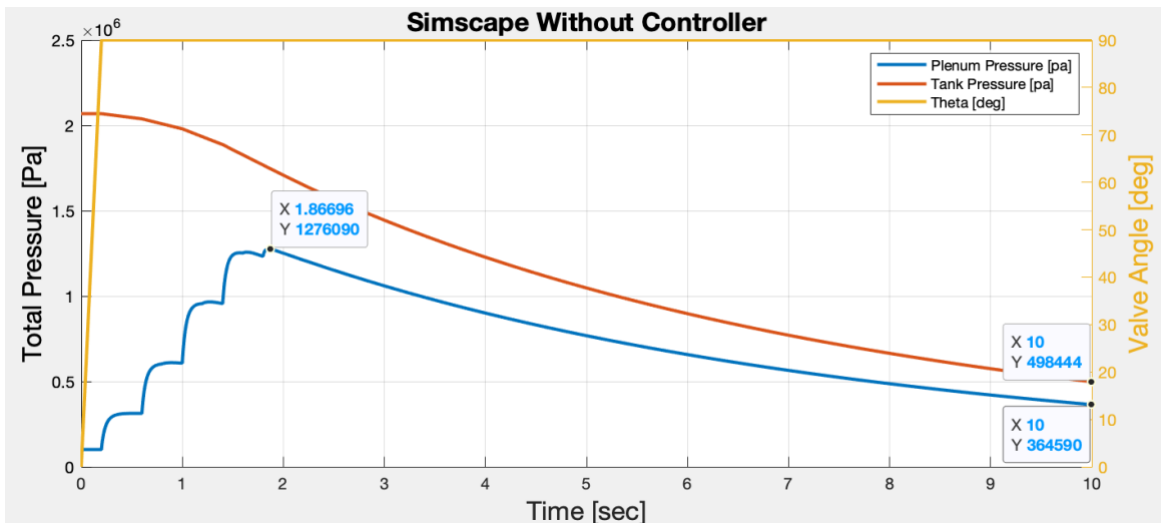


Figure 5. 28 Closed-loop response of Simscape BSWT without a controller

# Chapter 6 - Tuning and Validation of the PID Controller

      This chapter will describe how the PID controller gains are obtained and tuned to meet the design performance. Tuning controller gains is iterative and time-consuming in nature. To start with, the second method of the Ziegler-Nichols tuning technique will be applied first to get an educated guess for the gain values. Based on the insight of the finding, a series of fine tunings on the controller gains of $K_p$, $T_i$, and $T_d$ will then follow until the performance of the controller design is satisfied.

## 6.1 Controller Gains from Ziegler-Nichols

      The first step in the Ziegler-Nichols tuning rule is to find the sustainable oscillation period, $P_{cr}$, of the system by setting $T_i = \text{inf}$ and $T_d = 0$ and increasing $K_p$ as described in Table 1.2, section 1.2.3.2, which is found to be around 0.8 sec. The system response from the controller set is shown in Figure 6.1 below.
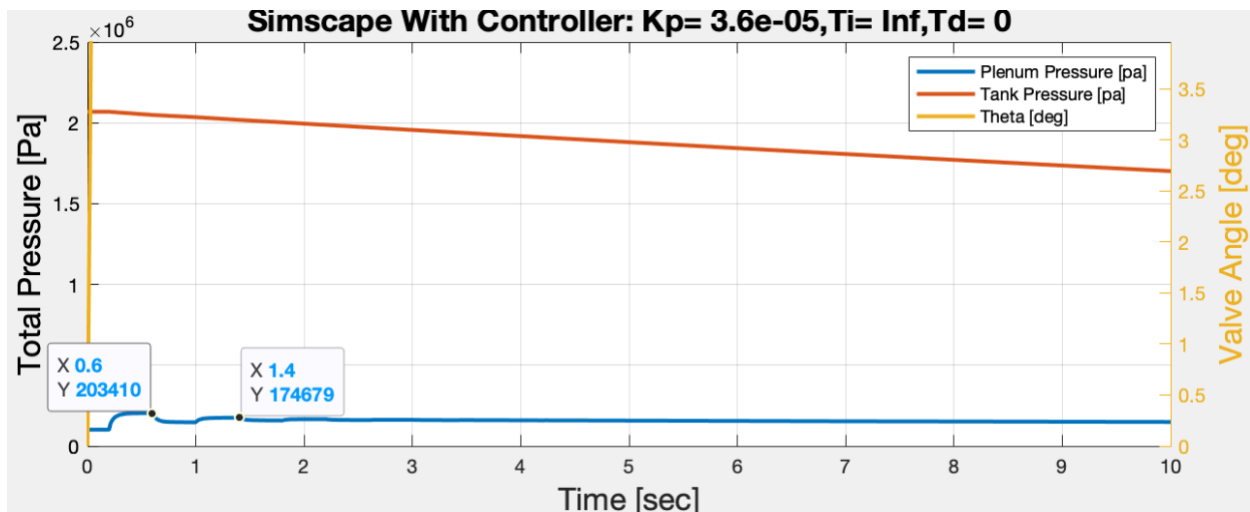


Figure 6. 1 System response with $K_p = 3.6e\text{-}5$, $T_i = \text{inf}$, and $T_d = 0$

      With $P_{cr} = 0.8$, the corresponding controller gains according to Table 1.2 are found to be: $K_p = 2.16e\text{-}5$, $T_i = 0.4$, and $T_d = 0.1$. Using these values, the responses of tank pressure, plenum chamber pressure, and valve angle are plotted together in Figure 6.2. It is noticed that although the system is stabilized by the control mechanism, the settling chamber pressure is much lower than the desired pressure. Also, there are multiple angle spikes along with the progress of the valve. Those sudden jumps of the valve angle could be due to the $T_d$ value and the use of the variable step size solver of the numerical integration, which probably would not be an issue when using a fix-step size in a real wind tunnel. Lastly, the plenum chamber pressure does not exhibit noticeable overshoot as expected from the Ziegler-Nichols method theoretically. Nevertheless, it is evident that the Ziegler-Nichols tuning method indeed provides a good starting point for fine-tuning.
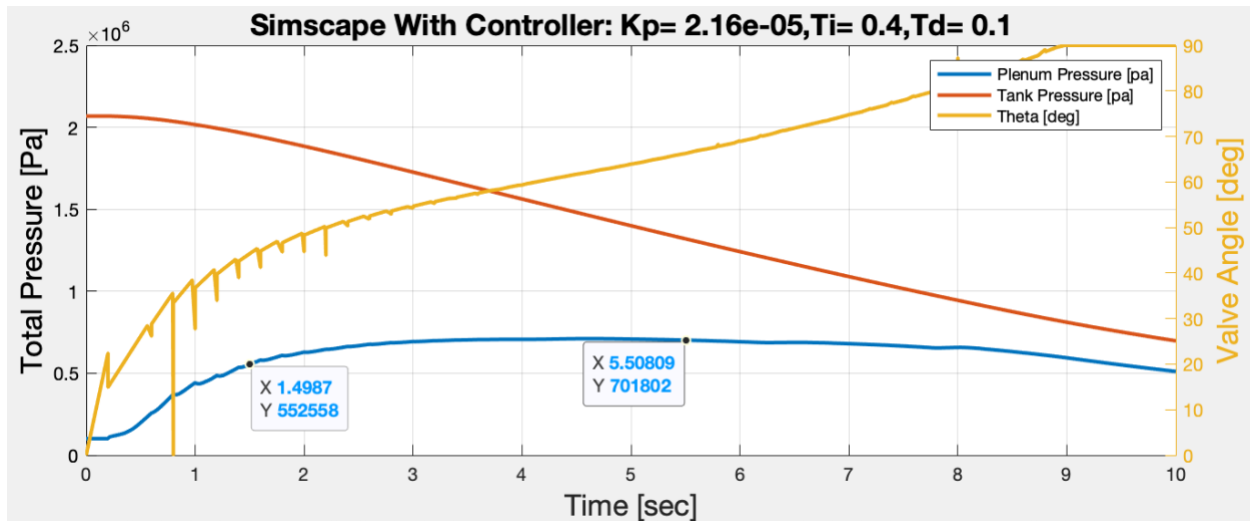
Figure 6. 2 System response with $K_p$ = 2.16e-5, $T_i$ = 0.4, and $T_d$ = 0.1

## 6.2 Tuning Controller Gains

Based on the responses of the system to the controller gains found from the Ziegler--Nichols tuning rule, it is observed that the rate change of the valve angle needs to be higher so that the flow passage can be opened up faster to bring the setting chamber pressure close to the desired set point to start the experiment. In addition to that, the transition of the valve angle needs to be smoother to better maintain the plenum chamber pressure. As aforementioned, the spikes of the valve angle could be due to the $T_d$ value and the variable step size. To minimize the noisy signal, $T_d$ gain is tuned low first to see its impact, which is shown in Figure 6.3. Compare Figure 6.2 and Figure 6.3, it can be seen that with a lower $T_d$ value used, the angle cusp has been diminished immediately.
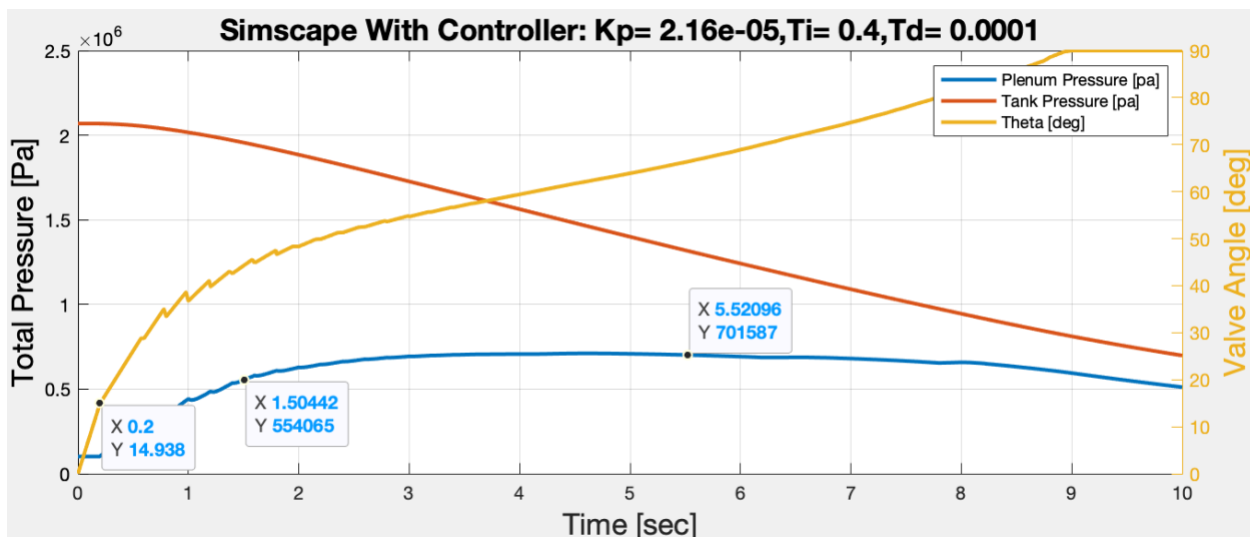


Figure 6. 3 System response with $K_p$ = 2.16e-5, $T_i$ = 0.4, and $T_d$ = 0.0001

## 6.2.1 Optimal Solvers

Notice that for code generated in real time, a fixed-step solver should be used to ensure the consistency of sampling time in real-time events. According to the documentation from Simscape modeling [39], it is recommended that a global variable-step solver and a local physical fixed-step solver should be used together. Therefore, in addition to the global Simulink solvers, the Backward Euler solver is selected as the local Simscape solver and the same sample time (deltaT = 0.01) used to develop the numerical algorithm described in chapter 3 is adopted in the Solver Configuration Simscape block. (refer to Figure 6.4 and 6.5). After the local solver is turned on, the same set of control gains is adopted to produce the system response, which is depicted in Figure 6.6. Compare Figure 6.3 and Figure 6.6, it is observed that with the evenly discretized step size of 0.01 sec, the evolution of valve angle rises from 0 to about 15 degrees within 0.01 sec and becomes very smooth afterward.
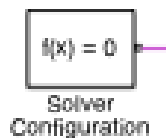


Figure 6. 4 Simscape block: Solver Configuration
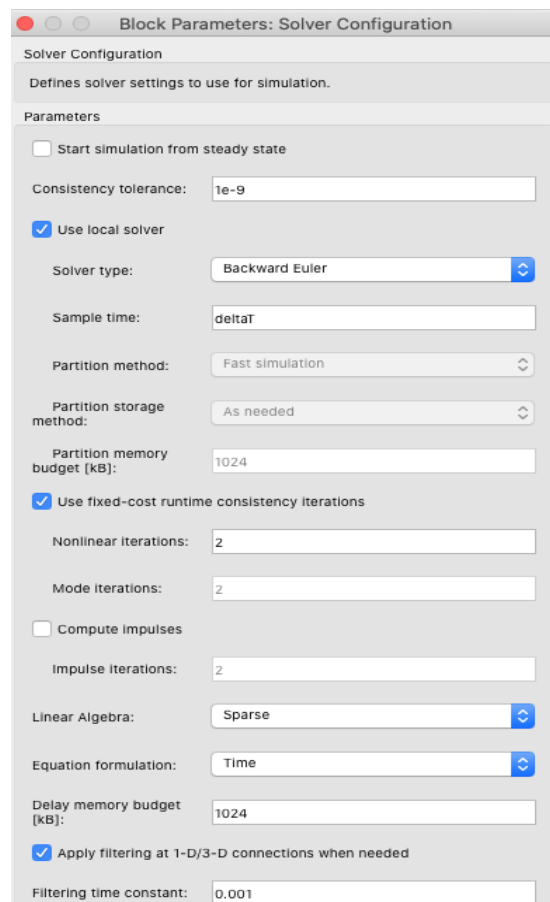


Figure 6. 5 Local solver configuration
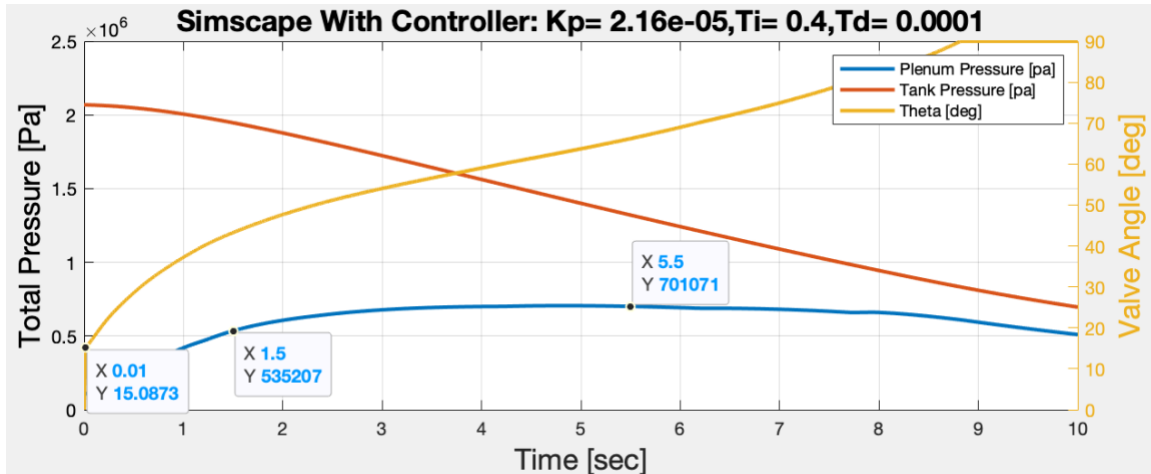
Figure 6. 6 System response with $K_p$ = 2.16e-5, $T_i$ = 0.4, and $T_d$ = 0.0001 when the global and local solvers are used simultaneously

## 6.2.2 Validation of Controller Gains

Through empirical approaches, it is found that the plenum chamber pressure can be maintained roughly constant with ± 1% error by many sets of controller gains. Figures 6.7, 6.8, and 6.9 below are the responses of the numerical algorithm and the Simscape model to three selected sets of controller gains respectively.
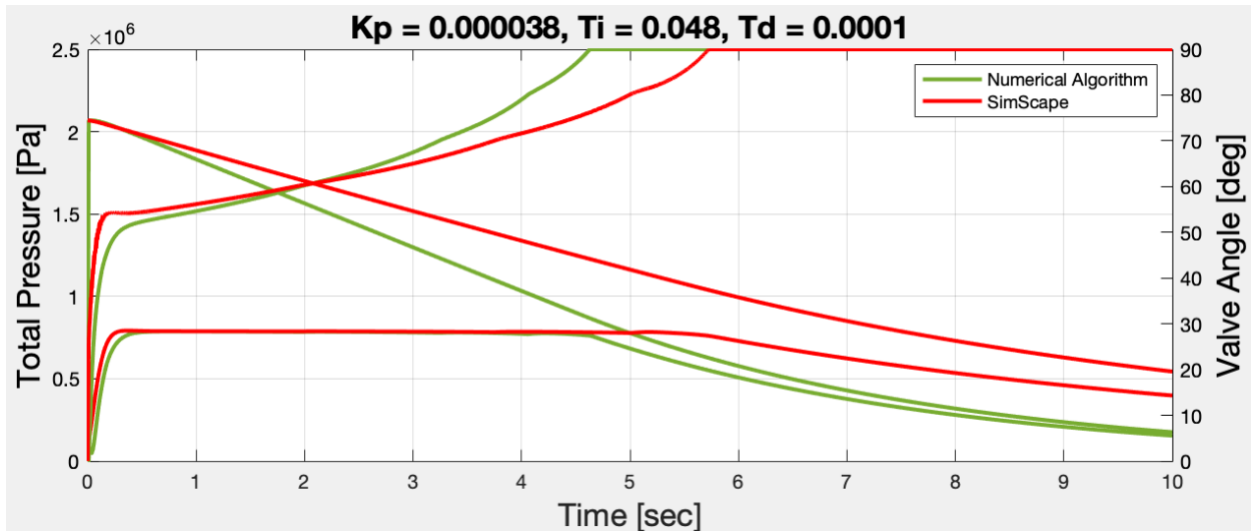


Figure 6. 7 System responses with $K_p$ = 3.8e-5, $T_i$ = 0.048, and $T_d$ = 0.0001
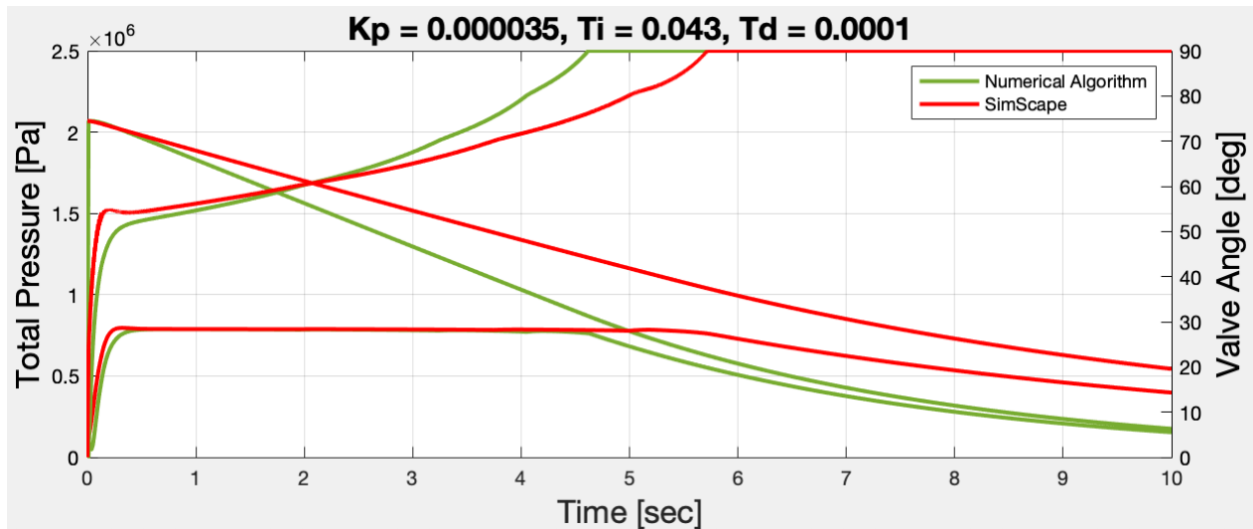
Figure 6. 8 System responses with $K_p$ = 3.5e-5, $T_i$ = 0.043, and $T_d$ = 0.0001
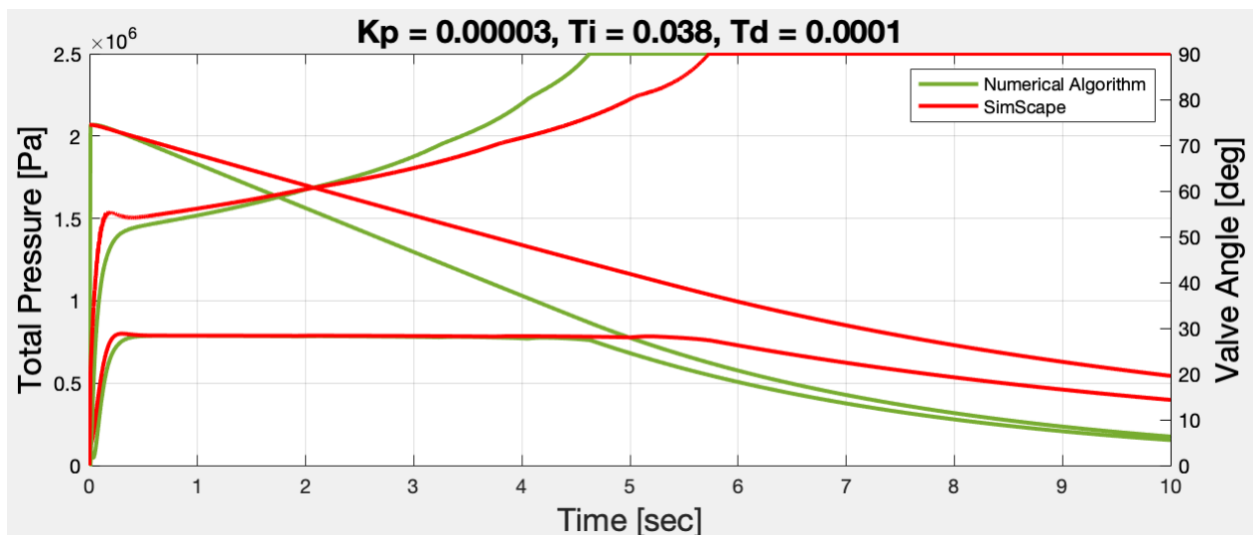


Figure 6. 9 System responses with $K_p$ = 3e-5, $T_i$ = 0.038, and $T_d$ = 0.0001

From Figures 6.7, 6.8, and 6.9, it is observed that the rate changes in tank pressure, plenum chamber pressure, and valve turning angle are all slower in the Simscape model than in the numerical algorithm. In addition, both the pressure and valve rise times are slightly faster from the Simscape model than from the numerical algorithm model. Also, the run time in the Simscape model is longer than that in the numeral algorithm. Another noticeable distinction is that the pressure difference between the tank and plenum chamber after the valve has fully opened is greater in the Simscape model than in the numerical algorithm, which is considered correct due to the finite filling time to the piping and settling chamber [2][14][40]. Lastly, the valve angle and settling chamber pressure overshoots only exhibit in the Simscape model. Despite these differences, the plenum chamber pressures in both models are well controlled and maintained at a constant level when implementing the same set of PID controllers.

## 6.3 Discussion

An air passage that is opened wide enough at the beginning of an experiment to immediately balance the pressure forces created from both sides of the control valve plays a critical role in run times. From chapter 2 the preliminary study, it is learned that if the initial cross-sectional area of the air passage is 0.0024 m$^2$, then the total run time for keeping a constant settling chamber pressure is around 6.6 seconds. Any delay in reaching this cross-sectional area will result in a shorter run time than 6.6 seconds, which is exhibited in both the numerical algorithm (approximate run time is about 4.6 seconds) and the Simscape model (approximate run time is about 5.6 seconds).

Ideally, the Simscape model should behave closely to the real physical wind tunnel. Providing that the Simscape model has fully captured the dynamics of the plant, the available run time from the Simscape model should be similar to the numerical algorithm. The possible causes for a longer run time from the Simscape model could be due to:

A. The omission of a sectional piping after the control valve:
   The length of the sectional piping used in the Simscape model is about 4 feet and the omission section is about 5 feet long as depicted in Appendix A. Without the implementation of this section, the finite filling time will not be accounted for, thus resulting in a longer experimental time available.
B. The settings of the geometric variables of the friction and heat transfer of the pipe element, such as:
   1) Internal surface roughness (or surface finish),which highly depends on how the components are manufactured. Smoother the surface, the less the pressure lost in the turbulent flow regime and longer the run time.
   2) Aggregate equivalent length of local resistances. Shortening this length will produce a longer run time.

In addition, it is expected there are some delays in the rise time due to the effects of finite filling time of the plenum chamber and the control valve lag [2]. However, such delay is not shown in the Simscape model. Practically, the LabView controller structure should be built around the valve angle theta increment (equation 3.16) and take in the real-time measurements of tank pressure, plenum chamber pressure, and valve angle from a data acquisition system as described in the paper [2]. However, there is neither real-time valve angle measurement, rotary ball valve, nor actuating motor in the Simscape model, which should all inject certain delays in the system. Thus, the resulting rise time is much faster than in reality. In general, a performance with such a faster rise time exhibited in both models may not be practicable. Even with the implementation of a booster that can swiftly open the valve within a second, industrial actuators equipped with such a high travel rate are very rare [2].

Despite the points discussed above, the settling chamber pressure can be maintained around a desired set point with various combinations of PID controller gain to achieve less than 1% pressure error. Table 6.1 tabulates the average pressure and the percent difference between the desired and sensing plenum chamber pressures when the system is controlled by selected sets of PID controller gains. The measuring time periods are from 1.5 to 5 seconds and from 1 to 5 seconds.

*Table 6. 1 Controller gains with pressure average and percent difference*

| Controller Gains | | | Measuring Frame: 1.5~5 [sec] | | Measuring Frame: 1~5 [sec] | |
|---|---|---|---|---|---|---|
| Kp | Ti | Td | Pressure Average [Pa] | % Difference | Pressure Average [Pa] | % Difference |
| 0.000038 | 0.048 | 0.0001 | 785,057 | 0.9888 | 785,413 | 0.9438 |
| 0.000037 | 0.046 | 0.0001 | 785,164 | 0.9753 | 785,516 | 0.9309 |
| 0.000034 | 0.043 | 0.0001 | 785,239 | 0.9913 | 785,395 | 0.9461 |
| 0.000036 | 0.044 | 0.0001 | 785,277 | 0.9610 | 785,625 | 0.9171 |
| 0.000035 | 0.043 | 0.0001 | 785,239 | 0.9658 | 785,589 | 0.9217 |
| 0.000033 | 0.042 | 0.0001 | 784,991 | 0.9971 | 785,351 | 0.9518 |
| 0.000032 | 0.040 | 0.0001 | 785,113 | 0.9817 | 785,468 | 0.9369 |
| 0.000031 | 0.039 | 0.0001 | 785,066 | 0.9876 | 785,423 | 0.9426 |
| 0.000030 | 0.038 | 0.0001 | 785,016 | 0.9939 | 785,375 | 0.9486 |

# Chapter 7 - Conclusion

A PID controller was designed successfully to effectively control the plenum chamber stagnation pressures required for Mach 2 tests for the BSWT at SJSU. During the preliminary study, the initial valve opening area and run time were surveyed to provide a preview of the pressure changes along the varying cross-sectional valve area as well as a justification of the need of a valve booster. A numerical algorithm was developed to orchestrate the evolutions of valve opening angle based on the specific type of rotary ball valve used at SJSU, the plenum chamber pressure difference, and the PID controller. Following the successfully built control mechanism, the physical BSWT was virtually constructed by using Simscape$^{TM}$ libraries in the Simulink$^{TM}$ environment to imitate HIL testing of the PID controller. From the second method of Ziegler-Nichols rules, the PID controller gains were first obtained and then were tuned manually to minimize the pressure error to be within 1 % for both numerical algorithm and the Simscape model. The responses of valve angles, tank pressure, settling chamber pressure were generated from the same optimized controllers, and the results and findings were discussed.

## 7.1 Limitations

Although it was concluded that the designed PID controller can sufficiently control the total pressure in the plenum chamber for Mach 2 tests, it is not vetted by experiments. Therefore, the optimized controller gains developed in this paper could best serve as reference values after the designed controller is applied to a LabVIEW program. After the installation of the controller, calibrations of the controller gains are required so that they can be fully integrated into the physical system of BSWT.

## 7.2 Future works

A few experiments need to be carried out after the completion of BSWT construction so as to validate both the mathematical model and the Simscape model. Once both models are validated, controller gains for different test conditions, Mach numbers, Reynolds numbers, etc. can be simulated offline in the virtual plant first to ensure the safety of wind tunnel operation, e.g. organ piping, as well as save energy and time required for a run.

# REFERENCES

[1]     Anderson, J. D., *Fundamentals of aerodynamics,*5th ed., McGraw-Hill, New York, 2010.

[2]     Braun, E., Lu, F., Panicker, P., Mitchell, R., Wilson, D., and Dutton, J., "Supersonic blowdown wind tunnel control using LabVIEW", Proceedings, *46th AIAA Aerospace Sciences Meeting and Exhibit,* Reno, Nevada, Jan. 2008.

[3]     Ilić, B., Miloš, M., Milosavljević, M., and Isaković, J., "Model-based stagnation pressure control in a supersonic wind tunnel," *FME Transactions,* Vol. 44, 2016, pp. 1-9.

[4]     Epple, P., Steppert, M., and Steber, M., "The impact of pressure regulators on the runtime and energy savings of supersonic blowdown wind tunnels," *Applied Mechanics and Materials,* Vol. 856, 2016, pp. 238-243.
        http://doi.org/10.4028/www.scientific.net/AMM.856.238

[5]     Matsumoto, J., Lu, F. K., and Wilson, D. R., "Preprogrammed controller for a supersonic wind tunnel," AIAA Paper 2001-1056, 2001.
        https://doi.org/10.2514/6.2001-1056

[6]     Wang, X., Li, S. Y., and Wang, Z. J., "Hierarchical Multiple Models Adaptive Decoupling Controller Applied to the Wind Tunnel System," *IFAC Proceedings,* Vol. 38, 2005, pp. 145-150.
        https://doi.org/10.3182/20050703-6-CZ-1902.00245

[7]     Lu, F. K., Wilson, D. R., and Matsumoto, J., "Rapid valve opening technique for supersonic blowdown tunnel," *Experimental thermal and fluid science,* Vol. 33, 2008, pp. 551-554.

[8]     Zurada, J. M., *Introduction to artificial neural systems*, Vol. 8, West Publishing Company, St. Paul, MN, 1992.

[9]     Wu, C-J, "Genetic Tuning of PID Controllers Using a Neural Network Model: A Seesaw Example," *Journal of Intelligent and Robotic Systems*, Vol. 25, May 1999, pp. 43–59.
        https://doi.org/10.1023/A:1008077610571

[10]    Motter, M.A, and Principe, J.C., "Neural control of the NASA Langley 16-foot transonic tunnel," *Proceedings of the 1997 American Control Conference*, Vol. 1, Albuquerque, NM, pp. 662–663.
        https://doi.org/10.1109/ACC.1997.611883

[11]    Kohonen, T., "The Self-organizing maps," *Proceedings of The IEEE*, Vol. 78, Sep. 1990, pp.1464-1480.

[12]    Nott, C. R., Ölçmen, S. M., Lewis, D. R., and Williams, K., "Supersonic, variable-throat, blow-down wind tunnel control using genetic algorithms, neural networks, and gain scheduled PID," *The International Journal of Artificial Intelligence, Neural Networks, and Complex Problem-Solving Technologies*, published online 15 Aug. 2007. https://doi.org/10.1007/s10489-007-0082-y

[13]    Shahrbabaki, A. N., Bazazzadeh, M., Shahriari, A., and Manshadi, M. D., "Intelligent controller design for a blowdown supersonic wind tunnel," *International Journal of Control and Automation*, Vol. 7, 2014, pp. 409-426. http://doi.org/10.14257/ijca.2014.7.1.37

[14]    Ilić, B., Miloš, M., and Isaković, J., "Cascade nonlinear feedforward-feedback control of stagnation pressure in a supersonic blowdown wind tunnel," *Measurement : Journal of the International Measurement Confederation*, Vol. 95, 2017, pp. 424–438. https://doi.org/10.1016/j.measurement.2016.10.046

[15]    Hwang, D-S, and Hsu, P-L., "A robust controller design for supersonic intermittent blowdown-type wind tunnels," *Aeronautical Journal*, Vol. 102, Issue 1013, March 1998, pp. 161–170. https://doi.org/10.1017/S0001924000065441

[16]    Andrei, N., "Blowdown wind tunnel control using an adaptive fuzzy PI controller," *INCAS Bulletin*, Vol. 5, 2013, pp. 89–98. https://doi.org/10.13111/2066-8201.2013.5.3.10

[17]    Krosel, S. M., Cole, G. L., Bruton, W. M., and Szuch, J. R., "A lumped parameter mathematical model for simulation of subsonic wind tunnels," NASA TM-87324, May 1986.

[18]    Visioli, A., "A new design for a PID plus feedforward controller," *Journal of Process Control*, Vol. 14, June 2004, pp. 457-463.

[19]    Ziegler, J. G, and Nichols, N. B., "Optimum Settings for Automatic Controllers," *Journal of Dynamic Systems, Measurement, and Control*, Vol. 115, June 1993, pp. 220–222. https://doi.org/10.1115/1.2899060

[20]  Ahamad, N., Uniyal, S., Sikander, A., and Singh, G., "A comparative study of PID controller tuning techniques for time delay processes," *U.P.B Sci. Bull. Series C Electr. Eng. Comput. Sci.*, Vol. *81*, 2019, pp. 129-142.

[21]  Fahmy, R. A., Badr, R. I., and Rahman, F. A., "Adaptive PID controller using RLS for SISO stable and unstable systems," *Advances in Power Electronics*. Vol. 2014, Oct. 2014.
https://doi.org/10.1155/2014/507142

[22]  Ogata, K., *Modern Control Engineering*, 4th ed., Prentice-Hall, Upper Saddle River, New Jersey, 2002.

[23]  Hall, N., "Normal shock wave equations," National Aeronautics and Space Administration," April 6, 2018.
https://www.grc.nasa.gov/www/k-12/airplane/normal.html

[24]  "brochure-fisher-vee-ball-rotary-control-valves-en-134994," 2018.

[25]  Fisher Control Valve, "What are the components of a Ball Valve?" YouTube, retrieved 23 March 2021.
https://www.youtube.com/watch?v=qOvbgVLjoK8

[26]  Weisstein, E., "Circle-Circle Intersection," WolframMathWorld, retrieved 21 March 2021.
https://mathworld.wolfram.com/Circle-CircleIntersection.html

[27]  Stewart, M., *Surface Production Operations: Volume III: Facility Piping and Pipeline Systems*, Elsevier Inc., Waltham, MA, Oct. 2015.
https://doi.org/10.1016/C2009-0-20127-9

[28]  Iqbal, K., *INTRODUCTION TO CONTROL SYSTEMS*, LibreTexts, Little Rock, AR, Nov. 2020.

[29]  Dykoff, M., "INTRODUCTION TO REGULATOR AND RELIEF VALVE SIZING".

[30]  "TECHNICAL - Emerson."
https://www.emerson.com/documents/automation/manuals-guides-complete-technical-section-fisher-en-140704.pdf

[31]  Thomas, P. J., "Appendix 3 Equations for control valve flow in SI units," *Simulation of industrial processes for control engineers*, Elsevier, Woburn, MA, 1999, pp. 342-343.

[32]    "Fisher High-Capacity Rotary Valves for General or Fibrous Slurry Service," May 2009.
https://usermanual.wiki/Emerson/EmersonFisherVeeBallV150UserGuide680595.595072
974.pdf

[33]    "Product Data Sheet - Catalog 12 Section 1 - Sept 2017," 2017.
https://www.emerson.com/documents/automation/product-data-sheet-catalog-12-section-
1-sept-2017-fisher-en-122394.pdf

[34]    Fung, Y-T, Settles, G.S., and Ray, A., "Microprocessor Control of High-Speed Wind
Tunnel Stagnation Pressure," AIAA Paper 88-2062, 1988.

[35]    Documentation, MathWorks, "Simulink," 2021.
https://www.mathworks.com/products/simulink.html

[36]    Documentation, MathWorks, "Simscape Fluids," 2021.
https://www.mathworks.com/help/physmod/hydro/index.html

[37]    Documentation, MathWorks, "Modeling Gas Systems," 2021.
https://www.mathworks.com/help/physmod/simscape/ug/modeling-gas-systems.html

[38]    Documentation, MathWorks, "Pipe (G)," 2021.
https://www.mathworks.com/help/physmod/simscape/ref/pipeg.html

[39]    Documentation, MathWorks, "Making Optimal Solver Choices for Physical Simulation,"
2021.
https://www.mathworks.com/help/physmod/simscape/ug/making-optimal-solver-choices-
for-physical-simulation.html

[40]    Nazarian Shahrbabaki, A., Bazazzadeh, M., Shahriari, A., and Dehghan Manshadi, M.
"Enhancing the Supersonic Wind Tunnel Performance Based on Plenum Temperature
Control". *International Scholarly Research Notices*, *2014*.
http://doi.org/10.1155/2014/317049

# APPENDICES

# Appendix A: Supersonic Wind Tunnel Lab Top View Schematic



*Supersonic Wind Tunnel Lab*

*Top View Schematic*

**List of needed parts**
*3x 3" Gate valves*
*2x 10" Flanges*
*1x 4" Elbow*
*1x 4" Tee*
*5ft 3" Stainless steel pipe*
*7ft 4" Stainless steel pipe*
*3ft 10" Stainless steel pipe*
*2x 1" drain valves under the tanks*
*1x Pressure gage*

*Green: available components*
*Gray: needed components*
*Red: component not needed*

*Note:*
*There are 1x 3" and 2x 1" ports on the tanks that will not be utilized and need to be capped.*
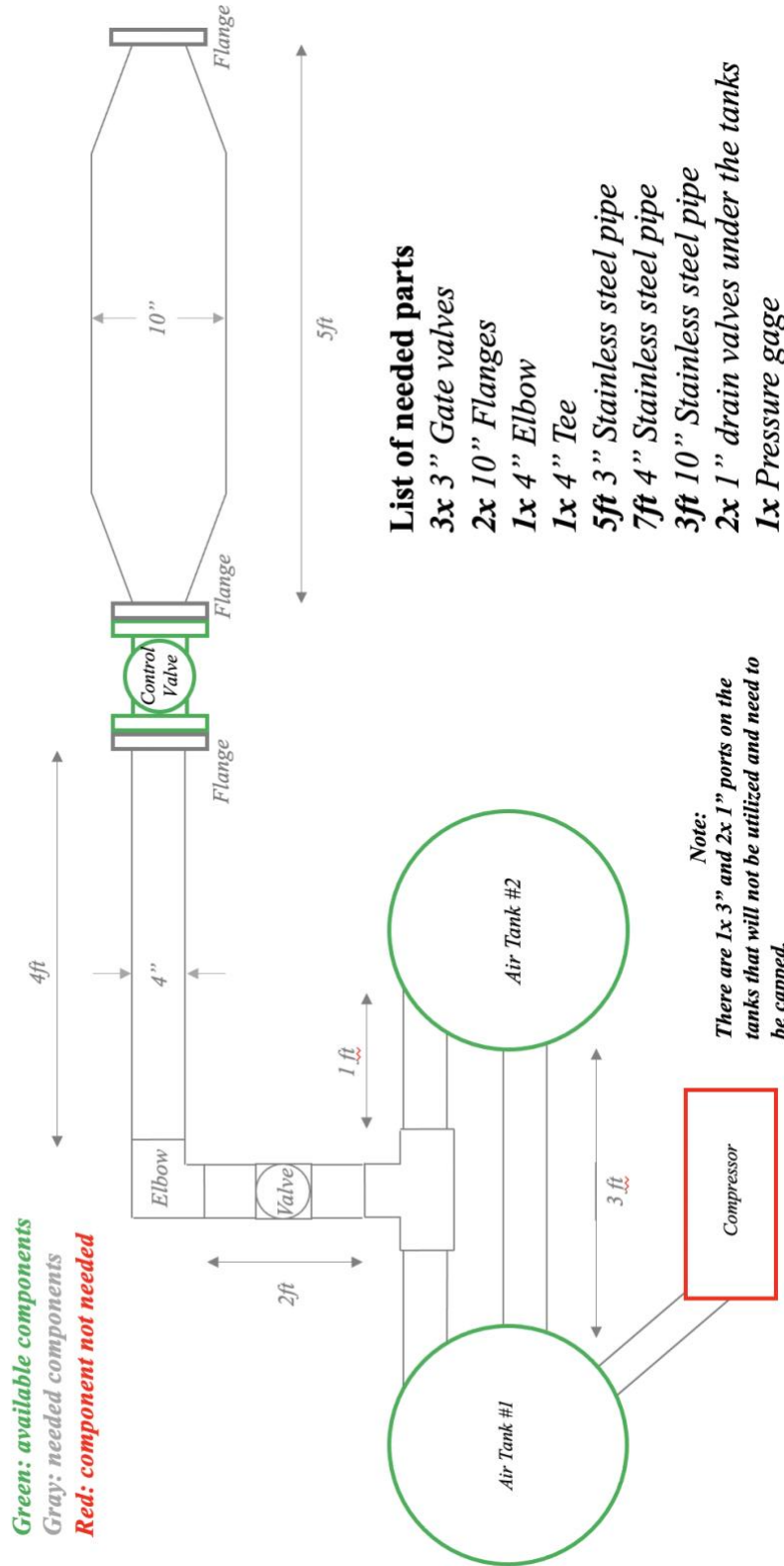
# Appendix B: Hanson Tank dimension
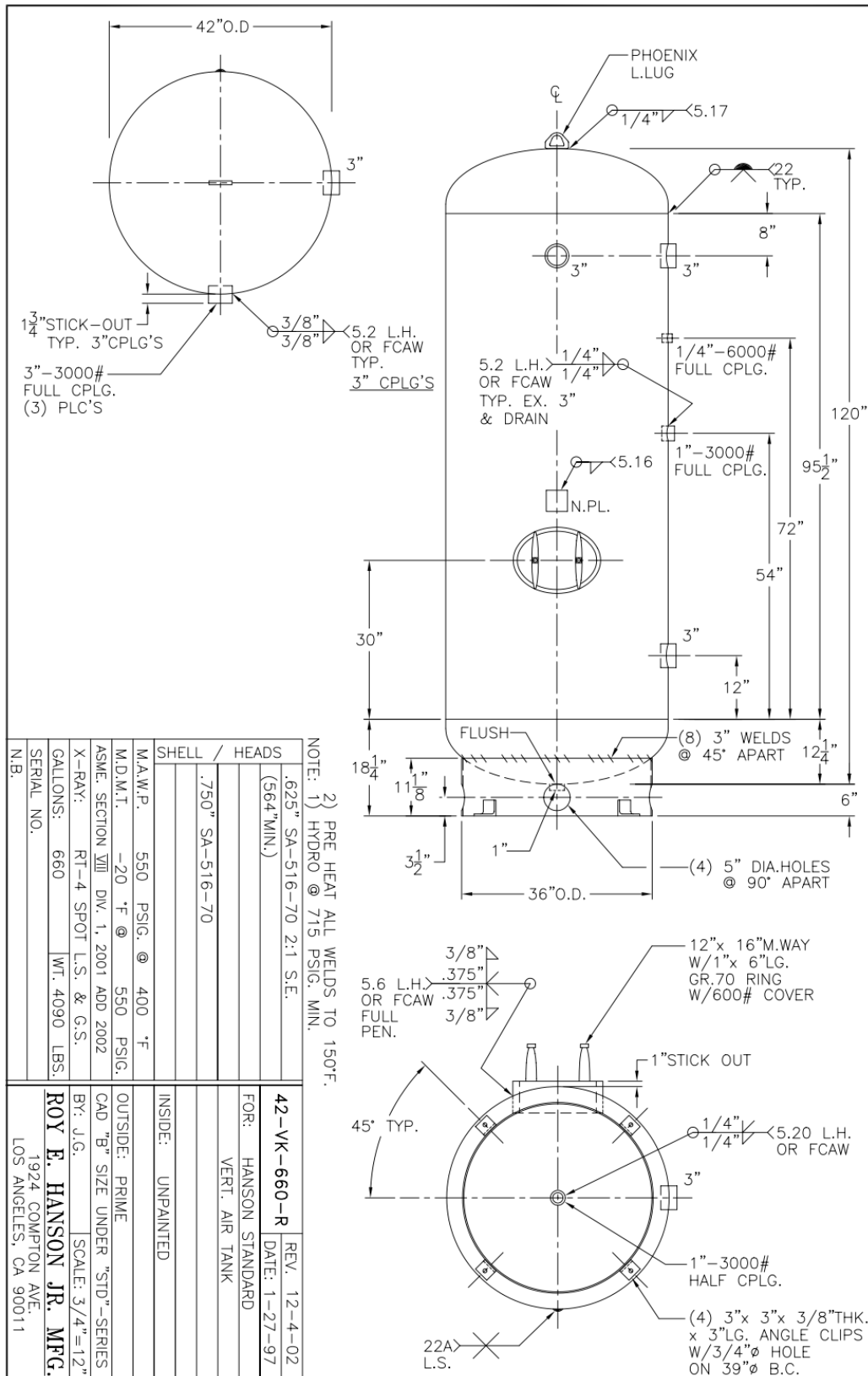
Appendix C: Matlab Script